Julia Messenlehner, BSc

Characterization of flavin-dependent oxidoreductases within the family of berberine bridge enzyme like proteins from *Arabidopsis thaliana*

MASTER'S THESIS

to achieve the university degree of

Master of Science

Master's degree programme: Biochemie und Molekulare Biomedizin

Submitted to

Graz University of Technology

Supervisors:

Prof. Dr. Peter Macheroux

Dr. Bastian Daniel

Institute of Biochemistry
Petersgasse 12/II
8010 Graz

Graz, March 2019

Gehalt ohne Methode führt zur Schwärmerei, Methode ohne Gehalt zum leeren Klügeln; Stoff ohne Form zum beschwerlichen Wissen, Form ohne Stoff zu einem hohlen Wähnen.

Johann Wolfgang von Goethe (1749 – 1832)

During the laboratory work in the course of my master thesis I learned a lot. I love science and its complexity and I want to thank all current and former members of the institute, my family and friends for their kind support.

EIDESSTATTLICHE ERKLÄRUNG

Ich erkläre an Eides statt, dass ich die vorliegende Arbeit selbstständig verfasst, andere als die angegebenen Quellen/Hilfsmittel nicht benutzt und die den benutzten Quellen wörtlich und inhaltlich entnommene Stellen als solche kenntlich gemacht habe. Das in TUGRAZonline hochgeladene Textdokument ist mit der vorliegenden Masterarbeit identisch.

Graz, am …… ……..

(Unterschrift)

STATUTORY DECLARATION

I declare that I have authored this thesis independently, that I have not used other than the declared sources/resources, and that I have explicitly marked all material which has been quoted either literally or by content from the used sources. The text document uploaded to TUGRAZonline is identical to the present master‘s thesis.

…… ……..

date (signature)

1 Abstract

Flavoproteins are a diverse class of enzymes that use flavin mononucleotide (FMN) or flavin adenine dinucleotide (FAD) as a cofactor and facilitate a large variety of catalytic tasks. Among the flavoproteins, the multigene family of berberine bridge enzyme-like (BBE-like) proteins is defined by the BBE(-like) domain (pfam 08031), which implicates a mono- or a unique bi-covalent attachment of the cofactor. Despite their frequent occurrence, little is known about the biochemical properties of these proteins, in particular with regard to their substrate range.

Recently, a member of this protein family from *Arabidopsis thaliana* named *At*BBE-like 15 has been identified as a monolignol oxidoreductase. To generate a deeper understanding of the role of this enzyme *in planta*, three groups from the fields of biochemistry, structural biology and plant physiology have teamed up. In this collaborative effort it was the aim of my master's thesis to identify the roles of amino acids in the active site in the course of monolignol oxidation.

To probe the catalytic mechanism of the enzyme, putative catalytic active residues were identified within the crystal structure (4UD8). Loss of function-variants were created by a site directed mutagenesis approach. A spectrophotometric assay was performed to evaluate the impact of the respective variations on the kinetic parameters of the enzyme as a function of pH.

For each variant, the pH optimum and the relative turnover number was determined. The strongest impact on the pH optimum was observed in the variants Q438V, Y139F and R292M with a ΔpH of +1.5, +1.2 and +1.2, respectively. The former two variants also showed the lowest residual activity with 4% and 1%, respectively while the R292M variant retains 50% of the activity.

Based on the structural information and the kinetic data the following mechanism is proposed: The catalytic machinery consists of the bicovalent attached FAD-cofactor, the catalytic base that activates the substrate by deprotonation (Y479) and the preorganized alkoxide binding site, formed by the amino acids Q438 and R292, which stabilize the negative charge prior to oxidation.

Since the active site composition is largely conserved within the family consisting of approximately 6000 members, the proposed mechanism for *At*BBE-like 15 can be considered a paradigm for the whole protein family.

2 Zusammenfassung

Proteine welche die redoxaktiven Kofaktoren Flavinmononukleotid (FMN) oder Flavin Adenindinukleotid (FAD) für die Katalyse verwenden werden Flavoproteine genannt.

Vertreter dieser Proteinfamilie finden sich in allen Organismen und katalysieren eine Vielzahl verschiedener und oft komplexer Reaktionen. Unter diesen Flavoenzymen findet sich in der Modellpflanze *Arabidopsis thaliana* (*At*) die Familie der Berberin Brücken Enzym-artigen (BBE-like Proteine) welche sich über ein Strukturelement, die BBE Domäne (pfam 08031) definieren und ihren Kofaktor FAD kovalent binden. Obwohl diese Enzyme und deren Verwandte in der Natur häufig zu finden sind, ist nur wenig über deren biochemische und physiologische Rolle in Pflanzen bekannt.

Ein Vertreter dieser Proteinfamilie aus *Arabidopsis thaliana, At*BBE-like 15, katalysiert die Oxidation von allylischen Alkoholen („Monolignole“) und wurde daher als Monolignoloxidoreduktase klassifiziert. Im Rahmen der Charakterisierung dieses Enzyms was es mein Ziel die Rolle der jeweiligen Aminosäurereste im aktiven Zentrum sowie den Mechanismus der enzymatischen Reaktion aufzuklären.

Die aus der Kristallstruktur (pdb code: 4UD8) eruierten aktiven Aminosäurereste wurden einzeln mittels ortsspezifischer Mutagenese ausgetauscht, um den jeweiligen Einfluss der veränderten Seitenkette auf die Katalyse zu untersuchen. Ein spektrophotometrischer Zugang wurde gewählt um die erzeugten Enzymvarianten auf ihre Aktivität im pH Bereich von 4 bis 9 zu untersuchen

Für jede Variante des Enzymes wurden das pH-Optimum und die Geschwindigkeit der Reaktion bestimmt. Der stärkste Einfluss auf das pH-Optimum wurde an den Positionen 438 (Glutamin), 479 (Tyrosin) und 292 (Arginin) detektiert mit einer jeweiligen Verschiebung von +1.5, +1.2 und +1.2 pH Einheiten verglichen mit dem ursprünglichen *At*BBE-like 15. Für die erst genannten Varianten wurde auch die geringste Restaktivität mit 4% und 1% festgestellt, wobei die R292M Variante 50% Restaktivität aufwies.

Ausgehend von diesen Daten und der Kristallstruktur schlagen wir einen Mechanismus für die Katalyse vor, in welchem das Substrat im ersten Schritt von Y479 deprotoniert wird. Die vorhandenen (partiellen) positiven Ladungen (R292 und Q438) stabilisieren das Alkoholat, bevor ein Hydrid zum Flavin übertragen wird und die Oxidation des Alkohols erfolgt.

Da die Zusammensetzung des aktiven Zentrums von *At*BBE-like 15 unter in etwa 6000 Mitgliedern dieser Proteinfamile stark konserviert ist, wird davon ausgegangen, dass dieser Mechanismus auch für andere Vertreter übernommen werden kann.

INDEX

List of abbreviations

6HDNO…6-hydroxy-D-nicotine oxidase
A40926...teicoplanin homolog
AknOx…aclacinomycin-N/aclacinomycin-A oxidase
AldO…alditol oxidase
At…*Arabidopsis thaliana*
*At*CKX…cytokinin dehydrogenase from *Arabidopsis thaliana*
BBE…berberine bridge enzyme
BG60…pollen allergen
CBDAS…cannabidiolic acid synthase
ChitO…chitooligosaccharide oxidase
CholOx…cholesterol oxidase
cnsA…aurantioclavine synthase
*Cp*ADHAPS...alkyldihydroxyacetonephosphate synthase from Cavia porcellus
Cv…*Chlorella variabilis*
*Dd*ADHAPS…alkyldihydroxyacetonephosphate synthase from *Dictyostelium discoideum*
DLDH…D-lactate dehydrogenase
DprE…decaprenylphosphoryl-beta-D-ribose oxidase
E22O…Ecdysteroid-22
EasE…chanoclavine synthase -oxidase
Ec…*Eschscholzia californica*
EncM…FAD-dependent oxygenase
EugO…eugenol oxidase
FAD…flavin adenine dinucleotide
FOX…flavin-dependent oxidoreductase
FsqB…fructosyl amino acid oxidase
GilR…pregilvocarcin V oxidase
GLDH…L-galactono-1,4-lactone dehydrogenase
GOOX…glucooligosaccharide oxidase
Ha-CHOX…*Helianthus annuus* carbohydrate oxidase
HOX…hexose oxidase
HPM9…alcohol oxidase from *Hypomyces subiculosus*
LaO…carbohydrate oxidase
LBA/LBZ…LB-medium with Ampicillin/Zeocin
Ls-CHOX…*Lactuca sativa* carbohydrate oxidase
Mp…*Marchantia polymorpha*
Mt…*Myceliophthora thermophile*
MurB…UDP-N-acetylenolpyruvoylglucosamine reductase
Nec5…nectarin 5
Nf…*Neosartorya fumigate*
Nt…*Nicotiana tabacum*
ONC… overnight culture
Pi…*Phytophthora infestans*
PCMH…p-cresol methylhydroxylase
Phl p 4…major pollen allergen (glucose dehydrogenase)
Pp…*Physcomitrella patens*
RPA1076…oxidoreductase from *Rhodopseudomonas palustris*
Sm…*Selaginella moellendorffii*
STOX…(S)-tetrahy- droprotoberberine oxidase
TamL...tirandymycin oxidase
THCAS...tetrahydrocannabinolic acid synthase
VAO…vanillyl-alcohol oxidase
Vc...*Volvox carteri f. nagariensis*
WT…wild type
XylO...xylooligosaccharide oxidase
*Zm*CKO2...cytokinin oxidase from *Zea mays*
*Zm*CKX1...cytokinin oxidase from *Zea mays*
DCPIP...dichlorophenol indophenol

3 Introduction

Flavoproteins are a diverse class of enzymes using derivatives of vitamin B2 – flavin mononucleotide (FMN) or flavin adenine dinucleotide (FAD) – as cofactor. The latter cofactor consists of an adenosine monophosphate connected via a phosphate and a ribityl to the redox active isoalloxazine ring. While the majority of flavoproteins binds their cofactor in a non-covalent manner, at least 10% feature a covalently attachment of their flavin cofactor [1]. This special tethering of the flavin cofactor was first discovered in succinate dehydrogenase and revealed a histidine residue covalently bound to the 8α methyl group of the isoalloxazine ring. There are four types of monocovalent FAD binding involving histidine, tyrosine or cysteine residues and one type of bi-covalent flavin binding namely the 8α-histidyl-6-S-cysteinyl-FAD [2]. This bi-covalent cofactor attachment was first discovered in glucooligosaccharide oxidase (GOOX) in 2005 [3] . Since then several enzymes with a bi-covalent FAD linking have been described and it was revealed that the tight interaction of the enzyme with the bi-covalently bound FAD gives rise to extraordinary high redox potentials (> +125 mV) compared to enzymes with monocovalent FAD binding (approximately -100 mV to +100 mV) or no covalent binding at all (-350 mV to 0 mV). This more positive redox potential gives rise to a more restricted selection of electron acceptors. Therefore, these enzymes with bicovalent FAD cofactor are often oxidases using dioxygen instead of dehydrogenases or reductases. It was also speculated that the bi-covalent attached FAD enables relatively open active sites for bulky substrates without cofactor dissociation and further increases the structural integrity of the enzyme [2]. Since no enzyme is described so far it is believed that the flavin binding is a posttranslational self-catalytic process [4]. The occurrence of this FAD binding and a specific hidden Markov model in the N-terminal part are characteristic properties and therefore a subfamily was defined as the berberine-bridge enzyme (BBE)-like (pfam entry PF08031) among the super family of FAD-linked oxidases (SCOPe d.58.32.2).

3.1 The berberine-bridge enzyme (BBE)-like proteins and their relatives

In Figure 1 the overall topology of the BBE-like proteins is shown as cartoon in panel A and the organization of the respective structural elements is represented in panel B.

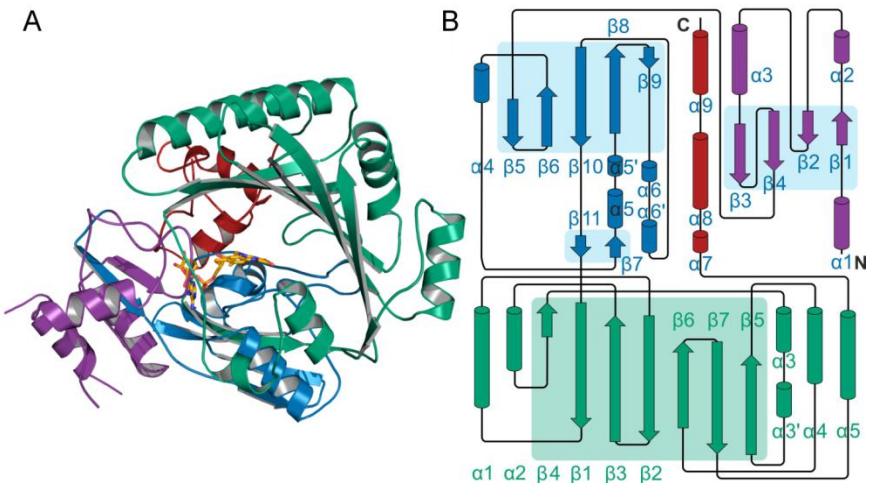

Figure 1: The overall topology of BBE-like proteins is shown in cartoon representation. B: Domain organization in *At*BBE-like 15 Individual subdomains of the FAD-binding module are colored in blue (C-terminal subdomain), purple (N-terminal subdomain) and red (BBE-domain). Opposed to the FAD-binding module the substrate-binding domain is located. At the interface the isoalloxazine ring is located and the active site is corporately formed by residues emerging from all domains. The figure was taken from [5]

The BBE enzymes are built up by a modular structure consisting of a N- and a C-terminal FAD-binding sub domain (colored in blue and purple, Figure 1) and a BBE-domain (colored in red) that are forming the FAD-binding module. Opposite to this, a module referred to as the substrate-binding domain is located (colored in green). The FAD-binding module formed by two sub domains harbors the residues responsible for the bi covalent attachment of the cofactor, the regulation of the oxygen reactivity of the enzyme, and the stabilization of the negative charge at the N1C2=O locus of the reduced flavin also emerge from the FAD-binding module. For a detailed description see Daniel *et al*. [5]. In contrast to this, the substrate binding domain is formed by a seven stranded antiparallel β-sheet that is covered with α-helices. C-terminal to the substrate-binding domain the BBE-domain is located that on the one hand establishing a connection between the N- and C-terminal sub domains of the FAD-binding module and on the other hand interacting with the ribityl chain and the N1C2=O locus of the isoalloxazine ring, which is located at the interface between the FAD-binding module and the substrate-binding domain. The active site of the enzyme is also formed at this interface, with all afore mentioned domains contributing to the active site. The active site is accessible from the surface by a funnel shaped channel, leading to the N5 position of the flavin with a putative catalytic base placed in the vicinity of the isoalloxazine ring.

The BBE- like proteins are named after the first and probably best studied member, the berberine bridge enzyme from *Eschscholzia californica* (Californian poppy), which catalyzes the oxidative ring closure of (*S*)-reticuline to (*S*)-scoulerine, a key reaction step in benzoylisoquinoline biosynthesis in the plant [6]–[8]. Other BBE-like proteins were found in fungi and bacteria, though plants still accumulate the highest number of BBE-like genes. In the course of elucidating the relatives and

probable ancestors of the BBE-like enzymes, a phylogenetic tree was created, which is depicted in Figure 2.

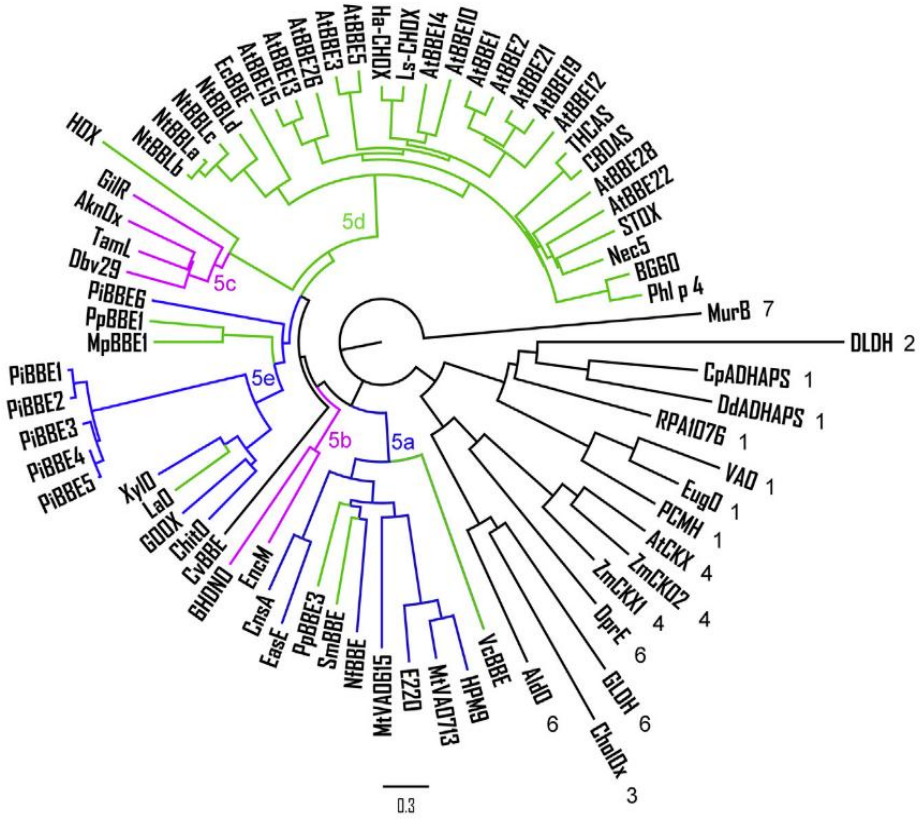

Figure 2: Phylogenetic tree of the superfamily of FAD-liked oxidases (SCOPe d.58.32). The numbering of the subfamilies is according to the SCOPe database and indicated at the branch tips except for BBE-like proteins (subfamily 5). The latter are colored according to their origin; BBE-like proteins from fungi, plants and bacteria are depicted in blue, green and violet, respectively. Subfamily 5 has been subdivided into clades 5a-d. The tree was created employing the sequences complied in Supplemental Table S1 as previously described [9] and visualized using iTOL [10]. The figure is taken from [5].

In the phylogenetic evaluation of the BBE-like proteins known so far and their close relatives like for example VAO [11], PCMH (p-cresol methylhydroxylase) [12] , EugO (eugenol oxidase) [13] or CKX (cytokinin dehydrogenase) [14] were considered. The BBE-likes from the kingdom of bacteria (clade 5c) are involved in the synthesis of antibiotics (galactono-lactone dehydrogenase GilR [15], tirandamycin oxidase TamL [16] , alcohol oxidase Dbv29 [17] and aclacinomycin oxidase AknOx [18], [19]). Enzymes from clade 5b were found to oxidize complex polyketides in the synthesis of the antibiotic myosmine in the case of EncM [20] while hydroxyl nicotine oxidase 6HDNO [21] is involved in the synthesis of a alkaloid related to nicotine. Enzymes that are found in fungi and are defined as clade 5e are involved in the oxidation of various oligosaccharides like XylO (xylooligosaccharide oxidase) [22], LaO (carbohydride oxidase)[23], GOOX and ChitO (chitooligosaccharide oxidase, UniProt: I1S2K2) while enzymes from clade 5a like EasE (chanoclavin oxidoreductase) [24] were found to catalyze ring closure reactions in the synthesis of alkaloids, E220 [25] is oxidizing an insect ecdysteroid upon infection, manipulating the hosts hormone system. Plants accumulate the highest

number of BBE-like genes. Their number even seems to correlate with the evolutionary stage of the plant species. Basal plants such as the moss *Physcomitrella patens* harbor 1-2 BBE-like genes whereas higher plants like the western poplar *(Populus trichocarpa*) accumulate up to 65 BBE-like genes [5]. It was also found that BBEs in plants are mainly involved in either the oxidation of alcohols and carbohydrates or in alkaloid biosynthesis [5], [26]. In *Arabidopsis thaliana* it was found that there are 27 genes coding for putative BBE-like proteins. Among the enzymes that act on alcohols, *At*BBE-like 13 and AtBBE-like 15 were identified as monolignol oxidoreductases. They accept cinnamyl-, *p*-coumaryl-, coniferyl- and sinapylalcohol as substrates and convert them to the corresponding aldehydes while reacting only slowly with molecular oxygen, i.e. are dehydrogenases rather than oxidases. Thus, it was assumed that these enzymes are involved in lignin biosynthesis, where they are likely to be responsible for the regulation of the aldehyde content of the lignin polymer [27]. The gene coding for flavin dependent oxidoreductase *At*BBE-like 3 was found to be upregulated in plant defense and the enzyme was found to oxidize an indole cyanohydrine to a carbonyl nitrile [28]. From the phylogenetic tree it was elucidated that this enzyme is related to oligoglucooxidases from lettuce (*Lativa sativa*) and sunflower (*Heliantus annuus*). It is shown by Custers *et al.* that both genes encoding for the enzymes are found to be upregulated after treatment of the plants with elicitors or during infection [29]. Enzymes involved in alkaloid biosynthesis among the BBE-like enzymes are BBL, Δ^9-tetrahydrocannabinolic acid synthase (THCAS) and cannabidiolic acid synthase (CBDAS) taking part of the conversion of nicotine in tobacco [30] and cannabinoids in cannabis sativa [31], respectively. BBE from *Eschscholzia califonica* mediates the oxidative ring closure of (*S*)-reticuline to (*S*)-scoulerine in the course of benzylisoquinoline alkaloid biosynthesis [32].

It was shown that two active site types, type I and IV are predominant in BBE-like proteins from plants (Figure 3) [5].

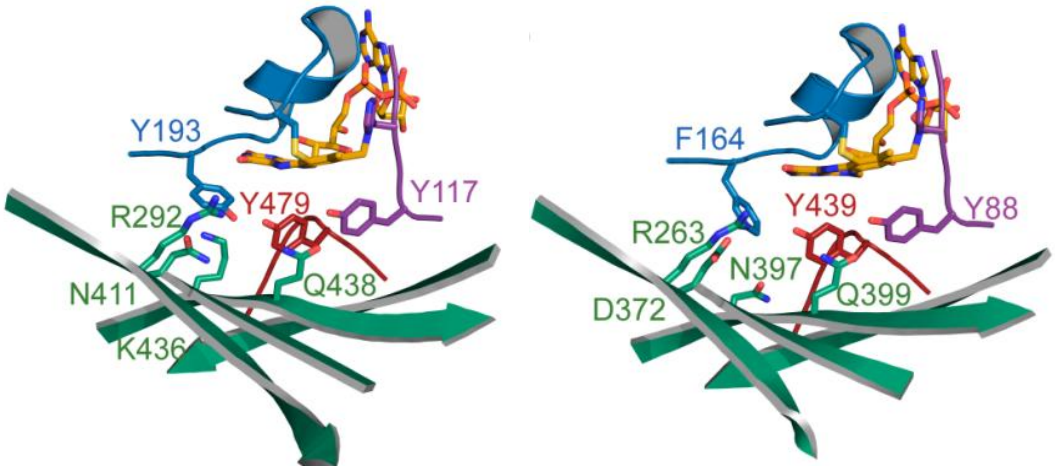

Figure 3: Frequently occurring active site types: A: Type I from *At*BBE-like protein 15 (pdb code 4UD8), B: Type IV from Phl p 4 (pdb code 4PWC). The figure was taken from [5].

The main difference in those two active site types is the nature and position of the catalytic base. While in type I, tyrosine residues Y193 and Y479 are proposed to act concertedly as catalytic base, in type IV, in type I a glutamic or aspartic acid substituting the base, while concurrently the residue corresponding to Y193 is a phenylalanine in type IV. A deprotonation of the remaining tyrosine by the carboxylic acid was proposed to activate the tyrosine to act as a catalytic base in order to initiate the hydride transfer. The interaction between Q438 and Y117 is found to be highly conserved in the catalytic machinery of BBE-like proteins. The active site type present in the monolignol oxidoreductase *At*BBE-like 15 is defined as Type I, which is the most abundant one in higher plants. Other enzymes sharing this active site type are AtBBE-like 13 and the putative monolignol oxidoreductase AtBBE-like 26, *At*BBE-like 3 (FOX1), and carbohydrate oxidases from sunflower and lettuce [28],[29]. Enzymes that share active site composition type IV are commonly from the kingdom of fungi or basal plants like for example GOOX, XylO, ChitO, LaO and the two pollen allergens PhI p 4 [33] and BG60 [34]. All afore mentioned enzymes do not only share a similar active site type but also a common reactivity towards oxidation of hydroxyl groups. The conservation of the residues forming the active site type I in enzymes from plants is summarized in Table 1.

Table 1: Conservation of the active site residues of BBE-like proteins in the plant kingdom. The sequences were fetched from the Pfam databank (BBE family: PF08031) in Viridiplantae. The conservation was surveyed by the aligned sequences using ClustalO. The numbering of the residues is according to AtBBE-like 15.

Residue	Conservation [%]	Proposed role in *At*BBE-like 15
H115	100	Bicovalent attachement of FAD
C179	92	Bicovalent attachement of FAD
Y479	92	Catalytic base
Y117	79	Polar contact to Q438
R292	74	Positive charge/Polar contact to N411V
Q438	74	Polar contact to Y193/polar contact to Y117
Y193	66	Catalytic base
K436	48	Cation-π-interaction with Y193
N411	45	Polar contact to R292, Q438 and Y193

The alignment of the amino acid sequence from the pfam database assigned to PF08031 in Viridiplantae resulted in the finding that Y479F is the most abundant residue among the analyzed proteins. With 92% it is as frequently found as the C179, which provides the bicovalent attachment of the FAD together with H115 (100% conserved). Other frequently found residues are Y117 and R292, Q438 with 79%, 74% and 74% abundance, respectively. While two thirds of the proteins harbour Y193, K436 and N411 are only found in 50% of the sequences.

3.2 AtBBE-like 26

In *Arabidopsis thaliana* the gene with the locus number At5g44400 encodes the berberine bridge enzyme-like protein 26. It was chosen for production in *Komagataella phaffii,* since it was shown by sequence alignment, that is has the highest amino acid sequence similarity to *At*BBE-like 13 and 15 and shares the same active site type and was therefore expected to be also a monolignol oxidoreductase. The predicted protein has a length of 537 amino acids including a signal sequence of 27 amino acids at the N-terminus as predicted by the signalP server [35]. The protein has a molecular mass of around 60 kDa and the theoretical isoelectric point was estimated to 9.7 for the stable protein by ProtParam from Expasy [36]. A homology model was created based on the structure of *At*BBE-like 15 using SwissProt [37] and the result is depicted in Figure 4.

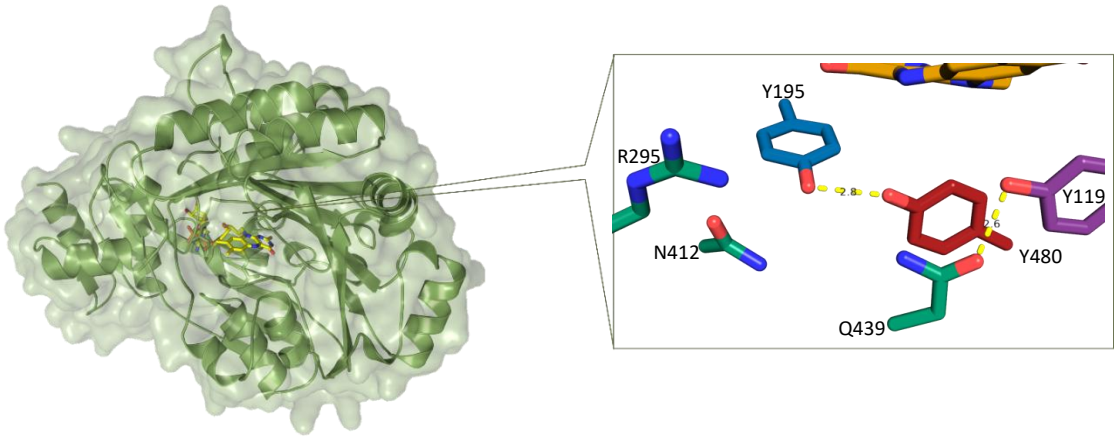

Figure 4: Homology model of *At*BBE-like 26 based on the crystal structure of *At*BBE-like 15 (63% sequence identity). In the left panel the overall topology of the enzyme with the yellow FAD cofactor is shown. In the right panel the most eminent amino acids in the active center are depicted. The bicovalent attachment to the enzyme is formed by a histidine to the 8α-position and a cysteine to the C6 position of the FAD. Y195 is assumed to be the catalytic base deprotonating the substrate.

3.3 *At*BBE-like 15

The gene *At*2g34790 in *Arabidopsis thaliana* genome encodes a flavoenzyme of this BBE-like family namely *At*BBE-like 15. It was heterologously produced in *K. phaffii* and crystallized by Daniel *et al*. (4UD8). It was also shown by Daniel *et al.* that the enzyme exhibits activity towards allylic alcohols, such as coumaryl- and coniferylalcohol, oxidizing the terminal alcohol group of the molecule to its corresponding aldehyde. *In planta*, they serve as monomeric building blocks, giving rise to a hydrophobic polymer in a radical polymerization mechanism, called lignin. It is hypothesized that the ratio of aldehyde to alcohol determines the physical properties of lignin in the plant. [27]

3.3.1 The active site of *At*BBE-like 15

In Figure 2 the active site dominated by polar residues and an extensive hydrogen bonding network is depicted. The residues are colored according to the sub domain they emerge from.

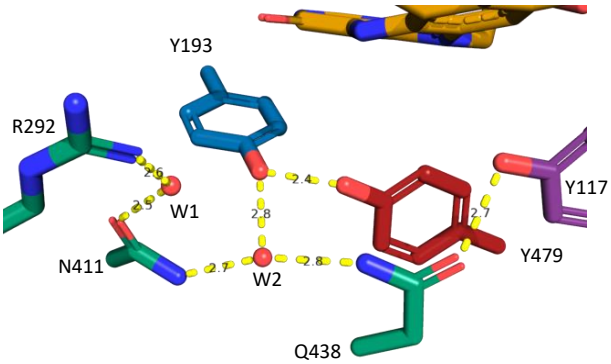

Figure 5: A: Overview of the amino acids building the active site of *At*BBE-like protein 15 (PDB 4UD8) with bicovalently linked FAD cofactor (yellow) and two water molecules (red spheres). The distances between polar contacts of the hydroxyl- and amine/guanidinium side chains and the two water molecules (W1 and W2) are indicated. K438 in close distance to the aromatic ring of Y193 is not shown for better overview.

The active site of *At*BBE-like 15 harbors seven amino acids forming a pocket in proper distance to a bicovalent linked FAD cofactor to take part in substrate oxidation. There are three "acidic" tyrosine residues (Y117, Y193 and Y479), a basic arginine (R292), a basic lysine (K438) and two polar amides, namely a glutamine and an asparagine. In the crystal structure, two water molecules are also found in the active site. Water molecule 1 (W1) is in hydrogen bonding distance to glutamine 438 (Q438) and tyrosine 193 (Y193) and the second water molecule, referred to as water molecule 2 (W2), is in hydrogen bonding distance to tyrosine 193 (Y193), arginine 292 (R292) and asparagine 411 (N411). The basic R292 provides a positive charge and it is thought to interact with the carbonyl group of the amide side chain of N411 via W2, whereas the amino group is proposed to form a hydrogen bond with W1. K436 is pointing towards the phenolic ring of Y193. In the crystal structure, K438 is in appropriate distance to the phenolic ring and in order to interact in a cation-π manner, thereby decreasing the pK_a by stabilizing the phenolic oxyanion and holding Y193 in place. The hydroxyl group of Y193 is located in the active site in close distance (2.4 Å) to the hydroxyl group of Y479. In previous studies, it was also proposed that these two amino acids may engage in a low barrier hydrogen bond. Additionally, it seems that there is a hydrogen bond between Y193 and W1 (2.8 Å). The glutamine at position 438 is also in hydrogen bonding distance to W1 and it is presumed that the hydroxyl group of tyrosine 117 forms a hydrogen bond to the carbonyl group of the amide side chain of Q438.

3.3.1.1 The low barrier hydrogen bond

The properties of H-bonds are predicted to vary with the distance between the H-donor and H-acceptor from >2.5 Å to ≪2.5 Å, in which the proton has become fully delocalized. The low barrier hydrogen bond (LBHB) lies between these states, with a distance in the range of 2.5 Å and the hydrogen is equally shared between its donor and acceptor [38]. LBHB occur when the p*K* values of the atoms sharing the proton are similar. The occurrence of so called low barrier hydrogen bonds in active sites of enzymes is frequently known and their contribution to catalysis has been discussed for

decades. Prominent representatives of enzymes using this kind of hydrogen bond are serine proteases, ketosteroid isomerases and citrate synthase [39] in acid-base catalysis. It was assumed that a "normal" hydrogen bond becomes a LBHB in the transition state or in a transient intermediate and the energy released in forming the LBHB is used to help lowering the activation barrier [40]. In a study of Wu *et al.*, it was questioned if the formation of the LBHB is causing the catalytic power of the enzyme but concluded that a π-conjugation gain in the tyrosine (catalytic base) stabilizes its deprotonation [41].

3.4 Aim of this work

Since the active site of plant BBE-likes is very conserved, elucidating the mechanism of aldehyde formation does not only mean to understand the catalytic mechanism of *At*BBE-like 15, but it does also provide deeper insights into the catalytic machinery of the whole family of BBE-like proteins. Our previous studies on *At*BBE-like 13 and *At*BBE-like 15 did not allow us to propose a detailed reaction mechanism for the conversion of either of these monolignols. Therefore, we applied a structure-guided mutagenesis program to elucidate the role of various polar active site residues. We generated the mutant genes by a site-directed mutagenesis, produced the variants in *Komagatella phaffii* and finally characterized them in terms of their activity as a function of the pH. A tight network of polar contacts and the presence of (partial) positive charges in the active site may tune the basicity of the catalytic base and the allylic alcohol and is also likely to establish a low barrier hydrogen bond.

3.4.1 Hypothesis

By combining the information obtained from the crystal structure solved by Daniel *et al.* (4ud8) and from the available literature, a catalytic mechanism was proposed, as shown in Scheme 1:

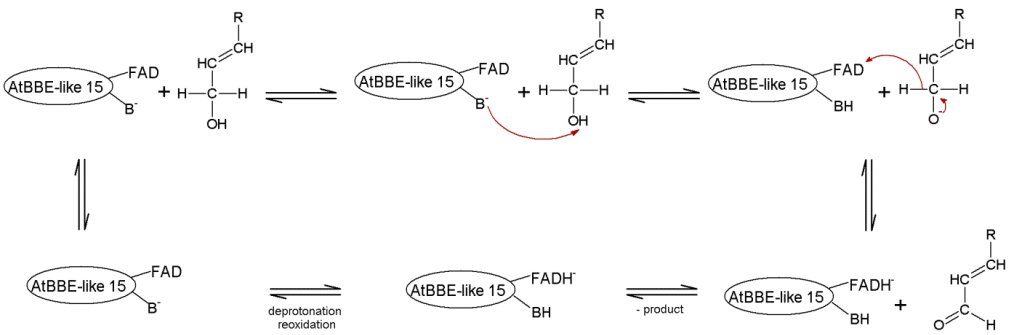

Scheme 1 Proposed order of the reaction. To facilitate oxidation of the alcohol, the substrate first needs to bind to the enzyme to form the enzyme substrate complex. The alcohol is activated upon deprotonation by an active site base to the corresponding alkoxide followed by the hydride transfer to the flavin cofactor and of the formation of aldehyde and reduced FAD. The natural electron acceptor for deprotonation and reoxidation of the enzyme remains unknown.

The hydroxyl group of Y479 is considered to form a hydrogen bond with Y193 and to stabilize thereby the latter's negative charge required for the deprotonation of the hydroxyl group of the substrate. It

is assumed that the partially positive character of the amide nitrogen of Q438 and N411 together with the positive charge of R292 enables the environment to tune the pK_a values of the (low barrier hydrogen bonded) acidic tyrosine residues and the alkoxide upon deprotonation prior to the formation of the planar, fully conjugated aldehyde, as it is depicted in Scheme 2.

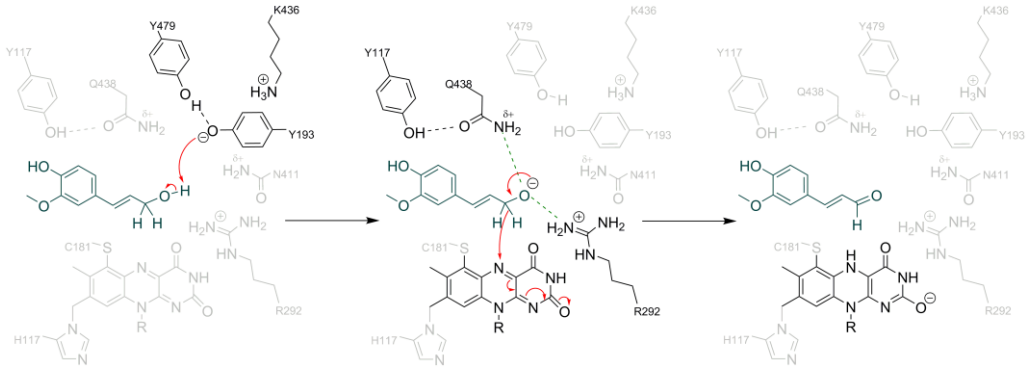

Scheme 2: Proposed reaction mechanism. The substrate is deprotonated by the catalytic base Y193. The corresponding alkoxide is stabilized by the (partial) positive charges of R292 and Q438 in the active site prior to the hydride transfer to the flavin cofactor and formation of the aldehyde product.

3.4.2 Approach

To gain information on the catalytic properties of a flavoenzymes, pre steady-state and steady-state kinetic approaches can be used. In a steady state experiment, a complete turnover process involving the reductive and the oxidative half reaction is analyzed, which allows the determination of the limiting rate. In the case of *At*BBE 15, a colorimetric assay was used to determine the pH optima and the limiting turnover rates of the wild type enzyme and several active site variants (Scheme 3).

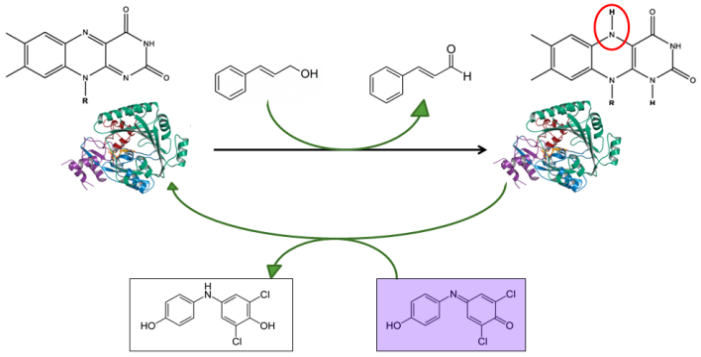

Scheme 3: Steady-state approach for the conversion of cinnamyl alcohol by AtBBE-like 15 with the final electron acceptor dichlophoenol indophoenol (DCPIP). The rate for the reduction of FAD is reflected by the decrease of the absorbance of DCPIP at 600 nm.

Additionally, pre steady-state experiments were performed in a stopped flow device in order to obtain the microscopic rate constants.

4 Material and methods

The experimental tasks were performed in the laboratories of the TU Graz, Petersgasse 12/II, from the 14th of January 2017 to August 2018.

4.1 Material

4.1.1 Devices

Table 2: Devices used

Device	Supplier		Used in/for
AGE Kit	SubCell® GT	Bio-RAD Lab. Inc., USA	
Autoclave	5075 MLV	Tuttnauer	
Centrifuges	Multifuge 3 s-r Sorvall® RC 6 plus Biofuge fresco	Heraeus Thermoelectron coop. Heraeus	Protein production and purification Eppendorf tube samples
Column			
Fermenter			
Glove box			
Heating block	TR-L 288	Liebisch	Eppendorf tube samples
HIS-trap column	HP, 1 mL, 5 mL	GE health care, UK	Protein purification
Ice machine	AF 200	Scotsman, USA	
Merckenschlager			
Microwave	-	Whirlpool Coop., USA	Agarose gel electrophoresis
Nanodrop	2000 UV- Vis	Thermo Scientific, USA	Quantifying DNA
Peristaltic pump	Dynamax, RP-1	Rainin Instruments, USA	Protein purification
pH-device	Orion star A211	Thermo Scientific, USA	
Scale	GP 3202 AG135	Sartorius, D Mettler Toledo	All day weighting Analytical scale
SDS electrophoresis Kit	Mini Protean™	BioRad Lab. Inc., USA	
Shaking fermenter	Multitron standard	Infors HT, CH	
Spectrophotometer	Specord® 200 plus U-1100	Analytic Jena, D Hitachi	Protein characterization OD measurement
Stopped-flow			
Thermocycler	2720 Compact	Applied Biosystems Eppendorf	Mutagenesis Eppendorf tube samples
Thermofluor®	CFX-Connect, Real time system	Bio-RAD Lab. Inc., USA	Protein characterisation
Thermostat	F12	Julabo	Photometer
Ultrasonic device	Labsonic® P	Sartorius, D	Protein purification
UV-Camera device	Gel Doc 2000	Biorad, USA	Agarose gel electrophoresis
Vortex	Vortex Genie 2	Scientific Ind. Inc., USA	

4.1.2 Chemicals

Table 3: Name, chemical formula, molecular weight in [g · mol^{-1}], CAS-Number and supplier of the used chemicals.

Name	Supplier	Used in/for
Acrylamide/BIS (N, N'-methylenebis-acrylamide)	$C_7H_{10}N_2O_2$, [154.17] CAS-No.: 110-26-9	Carl Roth GmbH, D
Agar-agar, Kobe I	-	Carl Roth GmbH, D
Agarose, Starpure	$C_{12}H_{18}O_9$, [306.27] CAS-No.: 9012-36-6	Starlab GmbH, D

Ampicillin	$C_{16}H_{19}N_3O_4S$, [349.41] CAS-No.: 69-53-4	
APS (ammonium persulfate)	$(NH_4)_2S_2O_8$, [228.18] CAS-No.: 7727-54-0	Carl Roth GmbH, D
Biotin	$C_{10}H_{16}N_2O_3S$, [244.30] CAS-No.: 58-85-5	
Boric acid	H_3BO_3, [61.83] CAS-No.: 11113-50-1	
Calcium sulfate dihydrate	$CaSO_4 \cdot 2H_2O$, [172.16] CAS-No.: 10101-41-4	
Cinnamyl alcohol	$C_9H_{10}O$, [134.17] CAS-No.: 104-54-1	
Citrate	$C_6H_8O_7$, [192.12] CAS-No.: 77-92-9	Carl Roth GmbH, D
Cobalt dichloride hexahydrate	$Cl_2CoH_{12}O_6$ [237.92] CAS-No.: 7791-13-1	
Coniferyl alcohol	$C_{10}H_{12}O_3$, [180.20] CAS-No.: 458-35-5	Sigma Aldrich, USA
Coomassie Brilliant Blue R-250	$C_{45}H_{44}N_3NaO_7S_2$, [825.97] CAS-No.: 6104-59-2	Carl Roth GmbH, D
Copper sulfate	$CuSO_4$, [159.60] CAS-No.: 7758-98-7	
Coumaryl alcohol	$C_9H_{10}O_{32}$, [150.17]] CAS-No.: 20649-40-5	
DCPIP (2,6-dichlorophenolindophenol)	$C_{12}H_7NCl_2O_2$**,** [268.1] CAS-No.: 956-48-9	Sigma Aldrich, USA
Dextrose	$C_6H_{12}O_6$, [180.16] CAS-No.: 50-99-7	
EDTA (ethylene diamine tetra acetic acid)	$C_{10}H_{14}N_2Na_2O_8 \cdot 2H_2O$, [372.24] CAS-No.: 6381-92-6	Carl Roth GmbH, D
Ethanol	C_2H_6O, [46.07] CAS-No.: 64-17-5	Carl Roth GmbH, D
FAD (flavin-adenine-dinucleotide disodium hydrate)	$C_{27}H_{31}N_9Na_2O_{15}P_2 \cdot H_2O$, [829.51] CAS-No.: 146-14-5	Sigma Aldrich, USA
Glycerol	$C_3H_8O_3$, [92.09] CAS-No.: 56-81-5	Carl Roth GmbH, D
Glycine	$C_8H_9NO_3$, [167.16] CAS-No.: 122-87-2	Carl Roth GmbH, D
HEPES (4-(2-hydroxyethyl)-1-piperazineethanesulfonic-acid)	$C_8H_{18}N_2O_4S$, [238.30] CAS-No.: 7365-45-9	Carl Roth GmbH, D
Hydrochloric acid conc. (12 M)	$HCl_{(aq),}$ [36.46] CAS-No: 7647-01-0	Carl Roth GmbH, D
Imidazole	$C_3H_4N_2$, [68.08] CAS-No.: 288-32-4	Carl Roth GmbH, D
Iron sulfate heptahydrate	$FeSO_4 \cdot 7H_2O$, [278.01] CAS-No.: 7782-63-0	
Isopropanol	C_3H_8O, [60.10] CAS-No.: 67-63-0	Carl Roth GmbH, D
Magnesium sulfate heptahydrate	$MgSO_4 \cdot 7H_2O$, [246.47] CAS-No.: 10034-99-8	
Manganese chloride tetrahydrate	$MnCl_2 \cdot 4H_2O$, [197.91] CAS-No.: 13446-34-9	
Methanol	CH_3OH, [32.04] CAS-No.: 67-56-1	
Milk powder	CAS-No.: 68517-61-4	Carl Roth GmbH, D

NaCl (sodium chloride)	NaCl, [58.44], CAS-No.: 7647-14-5	Carl Roth GmbH, D
Nickel sulfate hexahydrate	$NiSO_4 \cdot 6\ H_2O$, [262.8] CAS-No.: 10101-97-0	Sigma Aldrich, USA
Peptone	-	Bacto
Phosphoric acid	H_3PO_4, [97.99] CAS-No.: 7664-38-2	
Potassium dihydrogenphosphate	KH_2PO_4, [136.09] CAS-No.: 7778-77-0	
Potassium sulfate	K_2SO_4, [174.26] CAS-No.: 7778-80-5	
SDS (sodium dodecylsulfate)	$C_{12}H_{25}NaO_4S$, [288.37] CAS-No.: 151–21–3	Carl Roth GmbH, D
Sodium hydrogen phosphate	Na_2HPO_4, [141.96] CAS-No.: 7558-79-4	Carl Roth GmbH, D
Sodium iodide	NaI, [149.89] CAS-No.: 7681-82-5	
Sodium molybdate dihydrate	$H_4MoNa_2O_6$, [241.95] CAS-No.: 10102-40-6	
Sodiumhydroxid (NaOH)	NaOH, [39.99] CAS-No.: 1310-73-2	Carl Roth GmbH, D
Sorbitol	$C_6H_{14}O_6$, [182.17] CAS-No.: 50-70-4	
Sulfuric acid	H_2SO_4, [98.08] CAS-No.: 7664-93-9	
TEMED (tetramethylethylenediamine)	$C_6H_{16}N_2$, [116.21] CAS-No.: 110-18-9	Acros Organics, D
TRIS (tris(hydroxylmethyl) -aminomethan)	$C_4H_{11}NO_3$, [121.14] CAS-No.: 77-86-1	Carl Roth GmbH, D
TritonX	$C_{14}H_{22}O(C_2H_4O)_{9\text{-}10}$, [647] CAS-No.: 9002-93-1	
Tryptone/Peptone	-	Carl Roth GmbH, D
Yeast extract	CAS-No.: 8013-01-2	Carl Roth GmbH, D /Bacto
Zeocin	$C_{55}H_{86}N_{20}O_{21}S_2$, [1427.5] CAS-No.: 11031-11-1	
Zinc chloride	$ZnCl_2$, [136.32] CAS-No.: 7646-85-7	

4.1.3 Kits

Table 4: Kits used

Name	Supplier	Used in/for
Kit plamid isolation mini	Thermo Scientific, USA	
Kit plasmid isolation midi	Macherey Nagel, GER	
Gel purification	Promega, USA	
NucleoSpin® kit Plasmid QuickPure®	Macherey-Nagel, D	DNA purification
Protein assay solution	Bio-Rad	

Table 5: Components, suppliers and useage of additional utensils.

Name	Components	Manufacturer	Used in/with
5x HF buffer	-	Thermo Scientific, USA	Mutagenesis
6x DNA gel loading dye	-	Thermo Scientific, USA	Mutagenesis

Centriprep	10 000 Da cut off	Merck Millipore, USA	protein purification
Cuvettes	Quartz cuvettes Single use, 10 mm, 1.5 mL, PS	Hellma, D Brand, D	Protein spectra Every day use
dd H_2O	Ultra-Clear™	Siemens, D	
DNA standard	Gene Ruler™1 kb DNA Ladder	Thermo Scientific, USA	AGE
dNTPs	2 µM each	Thermo Scientific, USA	Mutagenesis
Paper filter	Cellulose 150 mm, 113P		Protein purification
Pipette tips	Blue Yellow White	Greiner bio-one, A	
Pipettes	100-1000 µL 50-200 µL 2-20 µL 0.2-2 µL	Gilson, F	
Protein standard	PageRuler™ Prestained Protein ladder	Thermo Scientific, USA	SDS-PAGE
HD-Green stain		Carl Roth GmbH, D	AGE
Syringe filters	Rotilabo® sterile, 0.22 µm	Carl Roth GmbH, D	Sterile filtration
Tubes	50 mL 15 mL 1.5 mL (sterilized) PCR (sterilized)	Greiner bio-one, A Greiner bio-one, A Eppendorf®	

4.1.4 Solutions

The amount of substances used in the different buffers is calculated according to the following basic formulas.

$$m = \frac{n}{M}$$

n…amount of substance [mol]
m…mass [g]
M…molar mass [g·mol^{-1}]

Equation 1: General equation for mass calculations.

$$c = \frac{n}{V}$$

c…concentration [M]
n…amount of substance [mol]
V…volume [L]

Equation 2: General equation for preparation of solutions.

$$c_1 \cdot V_1 = c_2 \cdot V_2$$

c_1…start concentration [M]
V_1…start volume [L]
c_2…final concentration [M]
V_2…final volume [L]

Equation 3: General equation for preparation of dilutions.

Table 6: Preparation and usage of solutions.* Sterile filtrated/autoclaved.

Reagent	Final conc.	Preparation		Used in
10x Dextrose*		80 g	in 400 mL dd H_2O	*K. phaffii* production
10x Yeast nitrogen base (YNB)*		60.3 g	In 450 mL dd H_2O	*K. phaffii* production
500x Biotin solution*		4 mg	In 20 mL dd H_2O	*K. phaffii* production
Ampicilin*	100 mg · mL^1			Gene production
Cinnamyl alcohol	5 mM		in 10 mL dd H_2O	Protein characterization
Coniferyl alcohol	10 mM	18 mg	in 10 mL dd H_2O	Protein characterization
DCPIP (stored at 4°C)	2 mM	5.8 mg	in 10 mL dd H_2O	Protein characterization
Destaining solution:				SDS-PAGE

Acetic acid EtOH dd H_2O	7.5% 20% 72.5%	75 mL 200 mL 725 mL	per 1 L solution	
Glycerol solution	50%	300 mL	in 300 mL dd H_2O	*K. phaffii* production
Milk powder solution	13%	6,5 g	in 500 mL TBST	Dot/Western blot
Nickel solution	0.1 M	13.14 g	In 1 L dd H_2O	Protein purification
Sorbitol*	1 M		In dd H2O	*K. phaffii* production
Staining solution: Acetic acid Ethanol Brilliant Blue R-250 dd H_2O	 7.5% 50% 0.25% 42.5%	 37.5 mL 250 mL 1.25 g 212.5 mL	 per 500 mL solution	SDS-PAGE
Zeocin*	50 mg · mL^{-1}			*K. phaffii* production

4.1.5 Buffers and media

Table 7: Preparation and usage of buffers and media. * Sterile filtrated/autoclaved.

Name	Ingredients	Final c	Preparation	Used in
10x Blotting buffer				western blot
50x TAE	TRIS/HCl EDTA Acetic acid	(2 M) 5242.28 g (0.05 M) 18.61 g (1 M) 60.05 g pH 8	in 1 L dd H_2O	AGE
5x SDS-PAGE gel sample buffer	TRIS/HCl (pH 6.8) SDS Glycerol DTT Bromphenol blue	250 mM 10% 30% 0.5 M 0.02%		SDS-PAGE
5x SDS-PAGE running buffer	TRIS Glycine EDTA SDS	15 g 71 g 1.68 g 2,5 g	in 1 L dd H_2O	SDS-PAGE
BMD medium	PPB, 2 M, pH 6 10x YNB Glucose 10x 500x Biotin	200 mL 100 mL 50 mL 2mL	+dd H_2O* to 1 L	*K. phaffii* screening
BMM10 medium	PPB, 2 M, pH 6 10x YNB 500x Biotin MeOH	20 mL 10 mL 0.2 mL 5 mL	+dd H_2O* to 100 mL	*K. phaffii* screening
BMM2 medium	PPB, 2 M, pH 6 10x YNB MeOH 500x Biotin	20 mL 10 mL 1 mL 0.2 mL	+dd H_2O* to 100 mL	*K. phaffii* screening
Elution buffer 10x	K_2HPO_4 NaCl Imidazole	(500 mM) 43.5 g (1500 mM) 43.8 g (100 mM) 3.4 g	Per 500 mL stock	Protein purification
LB -plates	Yeast extract NaCl Tryptone/Peptone Agar agar (Antibiotic)	2.5 g 2.5 g 5 g 7.5 g	in 500 mL dd H_2O	Plating
LB-medium	Yeast extract NaCl	5 g 5 g	in 1 L dd H_2O	Protein production

	Tryptone/Peptone	10 g		
Modified BSM medium	$CaSO_4 \cdot 2\ H_2O$ $MgSO_4 \cdot 7\ H_2O$ K_2SO_4 KOH NaCl Glycerol 85% H_3PO_4 (add last)	0.17 g · L^{-1} 2.32 g · L^{-1} 2.86 g · L^{-1} 2.00 g · L^{-1} 0.22 g · L^{-1} 32.23 g · L^{-1} 38.2 mL	3 L (per fermenter)	*K. phaffii* Fermentation
PP buffer*	Potassium phosphate	2 M pH 6		*K. phaffii* screening
PTM1 solution_1*	NaI $Na_2MoO \cdot 2\ H_2O$ H_3BO_3 $CoCl_2 \cdot 6\ H_2O$ Biotin	0.016 g 0.04 g 0.004 g 0.146 g 0.04 g	In 100 mL dd H_2O	K. *phaffii* Fermentation
PTM1 solution_2*	$CuSO_4 \cdot 5\ H_2O$ $MnCl_2 \cdot 4\ H_2O$ $ZnCl_2$ $FeSO_4 \cdot 7\ H_2O$ H_2SO_4 conc.	1.2 g 0.59 g 4.0 g 13.0 g 1.0 g	In 100 mL dd H_2O	K. *phaffii* Fermentation
TAE-buffer				AGE
TBS	Tris/HCl NaCl	50 mM 150 mM pH 8		Dot/Western blot
TBST	Tris/HCl NaCl Triton	50 mM 150 mM 0.2% pH 8		Dot/Western blot
TRIS-buffer 1	TRIS HCl	(1.5 M) 36.3 g pH 8.8	in 200 mL dd H_2O	SDS-PAGE
TRIS-buffer 2	TRIS HCl	(0.5 M) 12.1 g pH 6.8	in 200 mL dd H_2O	SDS-PAGE
Wash buffer 10x	K_2HPO4 NaCl Imidazole	(500 mM) 43.5 g (1500 mM) 43.8 g (100 mM) 3.4 g	Per 500 mL stock	Protein purification
YP	yeast extract (bacto) peptone (bacto)	15 g 30 g	in 1350 mL dd H_2O	K. *phaffii* Medium

4.1.5.1 Preparation of plates

500 mL of medium for 20 plates is prepared and autoclaved. Under sterile conditions, antibiotics are added (1000x stocks) to the chilled solution if needed. The medium is poured into Petri-dishes under sterile conditions and stored at 4°C after hardening.

4.1.6 Cells, DNA and enzymes

Table 8: Cells used

Name	Supplier	Used in/for
E.coli TOP 10	Stratagene	Plasmid production
Komagataella phaffii PDI		Protein production

Table 9: DNA used

Name	Supplier	Used in/for
pJET	Thermo Scientific, USA	Gene preparation
pPICZα		Gene preparation
Mutagenesis primer		Mutagenesis

Table 10: Enzymes/Antibodies used

Name	Supplier	Used in/for
*Sac*I	Thermo Scientific, USA	Gene preparation
*Xho*I	New England Biolabs	Gene preparation
*Not*I	New England Biolabs	Gene preparation
Phusion Polymerase	Thermo Scientific, USA	Gene preparation
T4 Ligase		Gene preparation
Hind		Gene preparation
His-Tag (D3I10) Rabbit mAb	Cell Signaling Tech.	Dot/western blot
Anti Rabbit IgG HRP-linked	Cell Signaling Tech.	Dot/western blot

4.2 Methods

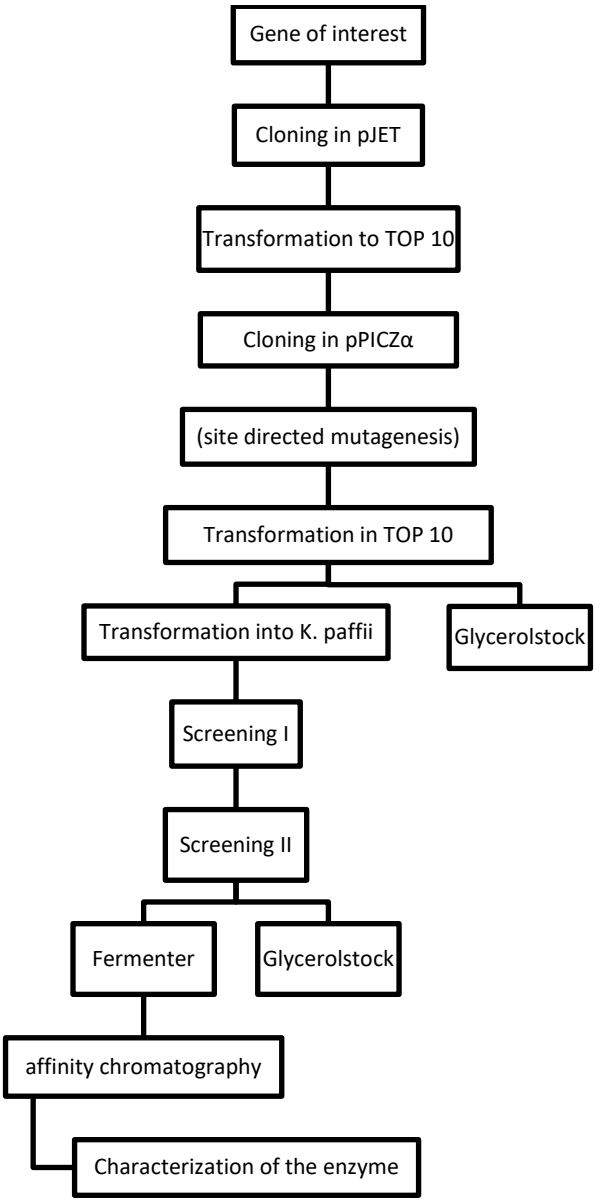

4.2.1 From gene to production vector

4.2.1.1 Design/purchase a gene for recombinant production

Companies like Thermo Fisher scientific provide an online platform to directly design the gene on their homepage prior to ordering. Before starting the sequence should be checked for signal peptides that can give rise to production problems in the non-native host. Then the sequence of interest is pasted as DNA or amino acid code. To facilitate protein purification it is favorable to integrate a histidine tag at the C-terminal end of the amino acid sequence. To prepare the gene for the recombinant production in *Komagataella phaffii* a part of a α-factor (nucleotide sequence AAAAGAGAGGCTGAAGCT) is pasted at the 5' end before the encoding sequence (the other part is

located on the pPICZα vector and the factor is reconstituted by ligation into the plasmid). On the outer end a 5‘ *Xho*I restriction site is integrated. On the 3‘ end a stop codon as well as a *Not*I restriction site are added.

4.2.1.2 Blunt end ligation of a gene with pJET vector

To assemble the purchased gene for production in a host organism, it is inserted into a pJET plasmid by blunt end ligation in the first. Therefore, the genes are dissolved in sterile dd H_2O to an end concentration of 100 ng · μL^{-1}. Next the ligation is prepared as listed in Table 11 and incubated for 20 min at 22 °C.

Table 11: Mixture for blunt end ligation of pJET and gene of interest

Reaction buffer (2x)	10 µL
pJET (blunt end)	1 µL
Gene (100 ng/µL)	2 µL
dd H_2O	6 µL
Ligase	1 µL
Total	20 µL

4.2.1.3 Transformation of *E. coli* TOP10 cells with pJET plasmid

Prepare: sterile LB-medium, competent TOP10 cells, LBA plates

To increase the number, the ligated construct is transformed with *E. coli* TOP10 cells via heat shock transformation. Therefore, 5 or 10 µL of the ligation mixture are added to 100 µL *E. coli* TOP10 chemical competent cells. First, the samples are incubated for 30 min on ice afterwards, they are heated at 42 °C for 2 min. 1 mL of sterile LB-medium is added immediately. Then the cells are incubated under shaking at 37 °C for at least 60 min to allow regeneration.

The regenerated samples are centrifuged at rpm_{max} for 30 sec. Under sterile conditions, the supernatant is decanted, the cell pellet is resuspended in the remaining liquid in the tube and pipetted on a LBA plate. A Drigalski-spatula is sterilized by flame and the sample is plated thoroughly. The plates incubated at 37 °C overnight.

4.2.1.4 pJET Plasmid isolation

Prepare: LBA plate, sterile LB medium, ampicillin

To increase the number of transformants, isolated colonies from overnight incubation are chosen from the LBA plate, picked up and streaked out on a fresh LBA plate. The plates incubated at 37 °C overnight. To isolate the plasmid DNA from an *E. coli* TOP10 strain (plate or glycerol stock), two ONCs are prepared in 5 mL sterile LB-medium in the afternoon. Ampicillin (100 mg · mL^{-1}) is added to an end concentration of 100 mg · L^{-1}. The medium is inoculated with cells from the plate and the ONCs are grown at 37 °C and 150 rpm overnight. The next morning 3 mL of the ONC are harvested by centrifugation at 4500 rpm for 15 min. The supernatant is discarded and the plasmid is isolated from

the cell pellet using the Miniprep Kit provided by Thermo Scientific. The DNA concentration and purity is controlled via Nanodrop.

4.2.1.5 Restriction of a gene

To equip the gene with sticky ends a restriction digestion is performed. The sample is mixed according to Table 12 and the sample is incubated at 37 °C overnight

Table 12: Mixture for restriction of pJET plasmid

Isolated DNA	43 µL
Cut-smart buffer	5 µL
*Xho*I (-HF)	1 µL
*Not*I (-HF)	1 µL
Total	50 µL

4.2.1.6 Purification ovf a gene by AGE and Kit

An agarose gel is prepared and the entire digested sample is loaded onto the gel. After the separation of the vector and the gene by electrophoresis the gene band is cut out of the gel and purified with the gel purification kit from Promega (Wizard Kit).

4.2.1.7 Ligation of the restricted gene with pPICZα

To ensemble the gene of interest with a vector the amount of insert is calculated using Equation 4 and the sample is mixed according to Table 13.

Equation 4: Calculation on the amount of insert for ligation of pPICZα.

$$m_i = \frac{m_v \cdot bp_i}{bp_v} \cdot n$$

with

m_i...mass of insert [ng]
m_v...mass of vector [100 ng]
b_{pi}...number of base pairs of insert
b_{pv}...number of base pairs of vector (pPICZα ~ 3.3 kbp)
n...times excess of insert (5-10)

Table 13: Mixture for ligation of pPICZα and gene of interest

Ligase buffer (10x)	2 µL
Insert (5-10 molar equivalents to vector)	x µL
pPICZα (100 ng)	y µL
Ligase	1 µL
Total (fill up with dd H_2O)	20 µL

The sample is incubated at 22 °C for 1 h. Afterwards the ligase is inactivated at 65°C for 10 min.

4.2.1.8 Transformation of *E. coli* TOP10 cells with pPICZα plasmid

Prepare: sterile LB-medium, competent TOP10 cells, LBZ plates

To increase the number of the prepared plasmid, it is transformed with *E. coli* TOP10 cells via heat shock transformation. Therefore, 20 µL of the ligation mix are added to 100 µL *E. coli* TOP 10 chemical competent cells. First, the samples are incubated for 30 min on ice afterwards, they are

heated at 42 °C for 2 min. 1 mL of sterile LB-medium is added immediately. Then the cells are incubated under shaking at 37 °C for at least 60 min to allow regeneration.

The regenerated samples are centrifuged at rpm_{max} for 30 sec. Under sterile conditions, the supernatant is decanted, the cell pellet is resuspended in the remaining liquid in the tube and pipetted on a LBZ plate. A Drigalski-spatula is sterilized by flame and the sample is plated thoroughly. The plates incubated at 37 °C overnight.

4.2.1.9 Plasmid isolation pPICZα

To increase the number of transformants, isolated colonies from overnight incubation are chosen from the LBZ plate, picked up and streaked out on a fresh LBZ plate. The plates incubated at 37 °C overnight. To isolate the plasmid DNA from an *E. coli* TOP10 strain, two ONCs are prepared in 5 mL sterile LB-medium in the afternoon. Zeocin (100 mg · mL^{-1}) is added to an end concentration of 100 mg · L^{-1}. The medium is inoculated with cells from the plate and the ONCs are grown at 37 °C and 150 rpm overnight. The next morning 3 mL of the ONC are harvested by centrifugation at 4500 rpm for 15 min. The supernatant is discarded and the plasmid is isolated from the cell pellet using the Miniprep Kit provided by Thermo Scientific.

4.2.1.10 Sequencing

The concentration of the plasmid DNA samples is determined by Nanodrop® to ensure a proper concentration for sequencing. LGC Genomics GmbH in Berlin, D., performed sequencing with 30 µL of samples with approximately 100 ng·$µL^{-1}$.

4.2.2 Site directed mutagenesis of WT plasmid

To elucidate the impact of single amino acids in the enzyme and the mechanism of the catalysis, single point mutations in the active site are introduced by site directed mutagenesis to probe the residual activity towards the substrate.

4.2.2.1 Design/purchase primers for site-directed mutagenesis

To introduce a mutation in a gene causing a single amino acid exchange, a site-directed mutagenesis is performed. To design primers for the PCR, Snap Gene Viewer is used. The primer length in total is at least 25-30 nucleotides with the mutation located in the center of the string. To introduce the point mutation the triplet codon of the relevant amino acid is altered using a codon sun. The sequence of the forward and the reverse primer should not overlap completely to prevent dimer formation. A melting temperature of 60-70 °C is desired which is checked by the online Thermo scientific melt temperature calculator using the sequence of the primer without the replaced nucleotides to gain information on the annealing temperature. The primers can be purchased from…

4.2.2.2 Plasmid isolation pPICZα

To increase the number of transformants, isolated colonies from overnight incubation are chosen from an LBZ plate, picked up and streaked out on a fresh LBZ plate. The plate is incubated at 37 °C overnight. To isolate the plasmid DNA from an *E. coli* TOP10 strain, two ONCs are prepared in 5 mL sterile LB-medium in the afternoon. Zeocin (100 mg · mL^{-1}) is added to an end concentration of 100 mg · L^{-1}. The ONCs are grown at 37 °C and 150 rpm overnight. The next morning 3 mL of the ONC is harvested by centrifugation at 4500 rpm for 15 min. The supernatant is discarded and the plasmid is isolated from the cell pellet using the Miniprep Kit provided by Thermo Scientific.

4.2.2.3 Sample preparation

The purchased primers, one forward (fw) and one reverse (rev) are suspended, as advised by the provider, in sterile dd H_2O to a final concentration of 100 µM. For the PCR reaction 200 µL of 10 µM dilutions of both primers are prepared. All mutagenesis samples are cooled permanently on ice. The samples are prepared as described in Table 14. As template the plasmid pPICαZ *At*BBE15 is used.

Table 14: Preparation of site directed mutagenesis samples.

Reagent	Fw [µL]	Rev [µL]	N [µL]
Sterile dd H_2O	38	38	37
Primer (1:20)	3 (fw)	3 (rev)	3 + 3 (fw + rev)
HF buffer 5x	5	5	5
dNTP Mix (2 mM)	1	1	1
Template (5-10 ng/µL)	2	2	-
Phusion Polymerase	1	1	1
Total	50	50	50

4.2.2.4 Site-directed mutagenesis – two step reaction

The samples are placed into the thermocycler and a program is created (see Table 15).

Table 15: Temperature program for the first step of mutagenesis.

		5 x			
T [°C]	95	95	60	68	68
Time	1 min	50 sec	50 sec	6 min	7 min
Step	initial denaturation	denaturation	annealing	extension	final extension

After the first step is finished, 25 µL of sample fw and 25 µL of sample rev are combined to a total of 50 µL. The samples are placed into the thermocycler and a program is created for the second mutagenesis step (see Table 16).

Table 16: Temperature program for second step of mutagenesis.

		18 x				
T [°C]	95	95	60	68	68	4
Time	1 min	50 sec	50 sec	6	7	-
Step	initial denaturation	denaturation	annealing	extension	final extension	storage

After the second cycle 5 µL of the sample are prepared for agarose gel electrophoresis testing. 1 µL of *Dpn*I is added to the sample and it is incubated at 37 °C for 3 hours.

4.2.2.5 Sequencing

The concentration of the samples is determined by Nanodrop® to ensure a proper concentration. Companies like LGC Genomics GmbH in Berlin, D., perform sequencing with 30 µL of samples with approximately 100 ng · μL^{-1}.

4.2.3 Production of protein in *Komagataella phaffii*

4.2.3.1 Plasmid isolation pPICZα

To increase the number of *E. coli* transformants, cells from glycerol stock are streaked out on a fresh LBA plate. The plate is incubated at 37 °C overnight.

To isolate the plasmid DNA from an *E. coli* TOP10 strain, two ONCs are prepared in 50 mL sterile LB-medium in the afternoon. Zeocin (100 mg · mL^{-1}) is added to an end concentration of 100 mg · L^{-1}. The ONCs are grown at 37 °C and 150 rpm overnight. The next morning the cells are harvested by centrifugation at 4500 rpm for 15 min. The supernatant is discarded and the plasmid is isolated from the cell pellet using the Midiprep Kit provided by Macherey and Nagel.

4.2.3.2 Transformation of pPICZα into *Komagataella phaffii*

Prepare: sterile electoporation cuvettes, sterile YPD, sterile Sorbitol 1 M, YPDZ (100-500 mg · L^{-1}) plates.

In the next step, the pPICZα plasmid is transformed in electrocompetent *Komagataella phaffii* PDI cells. For proper integration into the genome the plasmid has to be restricted to its linear form with *Sac*I. The purified plasmid is mixed with restriction enzyme as listed in Table 17 in the early afternoon and incubated at 37 °C overnight.

Table 17: Mixture for the restriction of the purified plasmid prior to transformation.

Purified DNA	50 µL
Buffer SacI	6 µL
*Sac*I	4 µL
Total	60 µL

The next day, the enzyme is inactivated at 80 °C for 20 min.

To desalt the sample preventing interruption of the electric circuit upon electroporation, a petri dish is filled with dd H_20 a filter is placed on the water surface and the sample is pipetted on it carefully. After 1.5-2 h the sample is removed again using a pipette. The sample is concentrated to 15-20 µL at 70 °C for 30 min or speedvac. The concentration of DNA and its purity (ratio 260/280 and 260/230) are determined by Nanodrop. 40 µL PDI-cells per transformation and a negative control are slowly thawed on ice. Additionally the UV-sterilized cuvettes are cooled on ice. The linearized plasmid DNA is added to the cells and the suspension is incubated on ice for 2-5 min. The cells are transferred to the bottom of the cuvettes by pipetting and knocking, the cuvettes are wiped dry on the outside and placed into the apparatus. The cells are pulsed with 1.5 kV and immediately 1 mL of YPD:Sorbitol (1 M), (1:1, vol:vol) are added (the time in milli seconds value displayed on the device gives an information on the sample conditions and is expected between 5-6). The cells are regenerated 2-3 h at 30 °C and 450 rpm in a thermomixer. 170 µL of the cell suspension are directly plated on YPDZ (100-500 mg · L^{-1}) plates and incubated at 30 °C for 2 days.

4.2.3.3 Protein production in dwp (screening I+II)

Prepare: rectangular YPDZ-plate (1000 mg · L^{-1}), sterile stocks of buffer, dd H_2O, biotin and 10x glucose, sterile deep well plate (dwp)

On Friday afternoon, 250 µL of BMD (Table 7) are transferred to each slot of a sterile 96 dwp. The colonies are picked from the plates and resuspended in the medium with pipette tips. One colony is used to inoculate 5 slots. The cultures are left to grow in a shaking incubator at 320 rpm and 28 °C for 2 days. Additionally, water filled dwp are placed in the incubator to prevent drying out of the cultures. On Monday morning a back-up plate is produced by stamping all 96 cultures on a single rectangular YPDZ (1000 mg · L^{-1}) plate. Afterwards, protein production is induced by adding 250 µL of BMM2 medium per slot. To keep the production level high 50 µL of BMM10 are added on Monday evening. On the next day the cells are provided with 50 µL of BMM10 medium in the morning and in the evening. On Wednesday morning the cells were harvested by centrifugation at 4000 rpm for 10 min. Then the supernatant is carefully transferred to a 96-well plate for activity testing and dot blot.

4.2.3.4 Preparation of glycerol stock

Cultures that are tested positive on his-tagged protein production are chosen for preservation and stored at -80 °C on glycerol. Therefore, an ONC is prepared in YPD without any antibiotic. The next day 2 stocks are prepared by suspending 1 mL of the ONC in 1 mL of 40 % sterile glycerol, respectively and incubated at room temperature for 1-2 hours. Afterwards the samples are frozen at -80 °C.

4.2.3.5 Protein production in fermenter

All BBE-like enzymes and all the variants described herein were expressed according to the following procedure.

4.2.3.5.1 Preparation of cells, media, solutions and fermenter

Preparation: sterile hoses and metal parts, bottle for MeOH (1 L), Inoculation flask, anti-foam, 1 L dd H_2O, Glycerol:H_2O 1:1 (1.2 L final volume in 2 L bottle), RTM solution, NH_3, H_3PO_4.

On Friday afternoon transformants from a glycerol stock are plated on YPDZ100-Agar medium and incubated at 30°C for two days. The YP media for the pre cultures is prepared (2x in 250 mL flask with 45 mL YP per fermenter, 2x 2 L baffled flasks with 270 mL YP per fermenter). All flasks are sealed with a cloth). The flasks are autoclaved and stored at 4 °C. 3 L of the growth media is prepared but sterilized in situ before inoculation of the fermenter. The fermenter is assembled with cooling water, foam sensor, over pressure valve, stirrer as well as pO2- and pH electrodes.

On Sunday morning the ONCs are prepared by adding 5 mL of sterile 10x dextrose and 50 µL of Zeocin (100 mg · mL^{-1}) to a final concentration of 100 mg · L^{-1} to 45 mL YP medium. The shake flasks

are inoculated using a pipette tip of the freshly grown cells from the plate and are incubated at 30 °C at 150 rpm overnight.

On Monday morning the pre cultures are prepared in 2 L flasks with 270 mL YP media and 30 mL of 10x dextrose. No Zeocin is added. The medium is inoculated using the freshly grown ONC to an OD_{600} of ~1 and incubated at 30 °C at 150 rpm until an OD_{600} of ~16 is reached assuming a doubling time of ~2 h. In the meanwhile the fermenter medium is transferred to the fermenter, the pH-sensor is calibrated and the fermenter is in situ sterilized. After cooling to 28 °C 15 mL of PTM are added and the acid, the base, the anti-foam and the glycerol:H_2O (1:1, w:w) stocks are sterile attached to the fermenter. The pH is set to ~4.5-5 and the oxygen sensor of the fermenter is calibrated (blank with N2 gas). The fermenter is inoculated sterile via an inoculums-flask equipped with the pre culture grown to an OD_{600} of ~16. The condition of the culture is controlled using MFCS Shell (stirring, pH, airflow, base, antifoam)

4.2.3.5.2 Growth of biomaterial and enzyme production

The glycerol fed batch is started slowly when the cells start to starve (pH is not decreasing anymore, stirring is decreasing). The flowrate is increased to provide 1 kg of glycerol in 24 hours at pH 5. To control the protein production with PAGE and western blot, 1 mL samples of the culture are taken subsequently and centrifuged at 10 000 rpm for 4 min at 4 °C. The supernatant is transferred to a fresh tube and the pellet and the supernatant are frozen separately. The next morning 5 mL of MeOH are provided directly by syringe and the glycerol feed slowly reduced and stopped within 2 hours. Also the pH is slowly increased to 6. Than the MeOH feed is started to provide 250 g in 24 hours.

4.2.3.5.3 Cell harvest

By the time the cells consumed 250 g of MeOH the feed is stopped. The pH is set to 8 with NaOH conc. and the cell suspension is transferred to 600-800 mL screw top centrifuge beakers equipped with a plastic bag inlet. The suspension is centrifuged at 5000 rpm at 4°C for 30 min.

4.2.4 Protein purification via Ni-affinity chromatography

4.2.4.1 Cell disruption (in case of failure in secretion *At*BBE26)

Since the complex structure of the yeasts cell wall, sonication is not efficient to break up the cells. Therefore, the frozen pellet is mixed 1:1 (w:w) with wash buffer and after thawing the protease inhibitors PMSF (1 M) and IC yeast are added 1:1000 and 1 µL per 10 mL respectively. Then the suspension is transferred to Merckenschlager screw-top flasks and zirconia beads are added (3:1, vol:vol). The suspension is homogenized for 3 min, cooling the samples with CO_2 gas flow every minute. The cell lysate is centrifuged at 18, 000 rpm for 30 min.

4.2.4.2 Affinity chromatography

Prepare: column material, buffer stocks, Biorad 1:5, DCPIP (2 mM), SDS-gels,

Equilibrated Ni-sepharose column material (15 mL) is added to the supernatant of the whole cell suspension or of the cell lysate in case of failure of secretion of the protein and slowly incubated under mild stirring at 4 °C for at least 1 hour. The loaded Ni-sepharose is then transferred to an empty column and sufficiently washed with wash buffer (K_2HPO_4:KH_2PO_4) and tested on protein content with qualitative Bradford assay. After washing, fractions of 5 mL are eluted and a DCPIP activity assay is performed in a 96-well plate. Subsequently samples for SDS-PAGE and western blot are taken (pellet, supernatant, wash and elution)

4.2.5 Cloning, Production and Purification controls

4.2.5.1 Agarose gel electrophoresis (AGE)

4.2.5.1.1 Preparation of AGE-gel

1 g of agarose is added to 100 mL of 1x TAE buffer and dissolved by heating in the microwave. Afterwards, the gel is cooled with water. 5 µL staining solution HD-Green Stain is added to the chilled mixture and the gel is casted. The comb is inserted and the gel is left to harden for ~30 min.

4.2.5.1.2 Electrophoresis

The gel is placed in the electrophoresis apparatus and is covered with 1x TAE buffer. The samples and the DNA standard are applied to the gel and the electrophoresis is started. For detection, the gel was carefully transferred to an UV-camera device and irradiated with UV-light.

4.2.5.1.3 AGE - control of mutagenesis

The agarose gel is prepared as described in section 4.2.5.5.1. The samples are prepared as described in Table 18. 12 µL of each sample and 5 µL of the DNA standard Gene Ruler™1 kb DNA Ladder are applied to the gel. Electrophoresis is run at 100 V for 35 min.

Table 18: Preparation of AGE - control of mutagenesis samples.

Sample	5 µL
dd H_2O	5 µL
6x loading dye	2 µL
Total	12 µL

4.2.5.1.4 AGE - control of plasmid purification

The agarose gel is prepared as described in section 4.2.5.5.1. The samples are prepared as described in Table 19. 12 µL of each sample and 5 µL of the DNA standard Gene Ruler™1 kb DNA Ladder are applied to the gel. Electrophoresis is run at 100 V for 35 min.

Table 19: Preparation of AGE - control of plasmid purification samples.

Plasmid	2 µL
dd H_2O	8 µL
6x loading dye	2 µL
Total	12 µL

4.2.5.2 Dot plot

To confirm the production and secretion of the his-tagged protein an antibody based immunoblot is performed. Therefore, a nitrocellulose membrane is wetted in TBS and then placed into a wet dot blot apparatus. All slots are filled with 600 µL of 1x TBS buffer which is then pulled through the membrane by applying vacuum. Then, 200 µL of cells supernatant is added to each position. After 10 min of incubation the supernatant is pulled through the membrane by applying vacuum. Each position is washed with 200 µL of 1x TBST. The membrane is removed from the apparatus and washed with 1x TBST for 10 min followed by 1 h of blocking with 15% milk powder solution in TBST at room temperature. Afterwards, the membrane is washed with 1x TBST for 5 min before incubation with anti-his antibody from rabbit (1:2000) in 2.5% milk powder in TBST at 4°C on a shaker overnight. The next day the membrane is washed 3x with TBST for 10 min before incubation with the HRP-linked anti-rabbit antibody (1:5000) in 2.5% milk powder in TBST for 1 hour. Afterwards, the membrane is washed 3x with TBST for 10 min and 1x with TBS for 5 min. For detection Luminol is mixed with H_2O_2 (1:1, vol:vol) and thoroughly applied on the membrane by pipetting. The signal is visualized on a photo film in the darkroom.

4.2.5.3 Activity assay in 96-well plate

To detect the *At*BBE-like protein in the supernatant or in the elution fractions after affinity chromatography a qualitative activity is performed using coniferyl alcohol as a substrate. Since a substrate for *At*BBE-like26 is not known yet it is also tested for activity on glucose, cellobiose and fructose.

Table 20: mixture for the master mix for testing the activity of the enzyme in 96-well plate qualitatively. *

Reagent	Volume [µL]
Buffer* (50 mM, pH 5-8)	1380
DCPIP (2 mM)	120
Coniferylalcohol (10 mM)	200
Total	1700

Table 21: mixture for testing the activity of the enzyme in 96-well plate qualitatively.

Reagent	Volume [µL]
Master mix	100
Supernatant/fraction	100
Total	200

4.2.5.4 Qualitative Bradford protein assay in 96-well plate

To check the total protein content in supernatant, wash or elution fractions Bradford solution provided by Biorad is used as listed in Table 22.

Table 22: Mixture for qualitative total protein assay in 96 well plates.

BIORAD™ 1:5 in dd H_2O	200 µL
Protein solution	10 µL

4.2.5.5 SDS-gel electrophoresis (SDS-PAGE)

4.2.5.5.1 Preparation of SDS-PAGE gel

Two plates are combined, placed into the casting apparatus and correct setting and tightness of the plates is ensured with H_2O. The separating gel and the stacking gel are prepared in 50 mL tubes (Table 23). The polymerization is started by adding APS directly before casting.

Table 23: Preparation of 1x 12.5% separating and 1x 5% stacking gel for SDS-PAGE; lin. separating region 12-60 kDa.

Acrylamide/BIS	1.56 mL	0.313 mL
1.5 M TRIS buffer pH 8.8	1.875 mL	-
0.5 M TRIS	-	0.313 mL
SDS 20%	25 µL	12.5 µL
dd H_2O	1.495 mL	1.845 mL
TEMED	5 µL	2.5 µL
10% APS	24 µL	12.5 µL

After the separating gel is casted, it is overlaid with BuOH and polymerized. BuOH is removed after ~10 min and the gel is washed with H_2O. After the stacking gel is casted above the separating gel, the comb is inserted. The polymerised gel is stored in wet paper towel and aluminum foil in the fridge (4°C).

4.2.5.5.2 Sample preparation PAGE-production check

The supernatant and the pellet samples that are taken subsequently from the culture in the fermenter are prepared for PAGE and western blot as listed in Table 24. The pellet is resuspended in 1 mL of dd H2O per 100 mg of cells.

Table 24: Preparation of PAGE production check samples.

Pellet sample	
Cell suspension	5 µL
dd H_2O	25 µL
4x sample buffer	10 µL
Total	40 µL

Supernatant sample	
supernatant	24 µL
4x sample buffer	8 µL
Total	32 µL

After mixing, the samples are heated at 98 °C for 10 min and spun down. 5 µL of the pellet sample and 10 µL of supernatant sample are loaded on the gel.

4.2.5.5.3 Sample preparation PAGE-purification check

The wash and elution fractions from affinity chromatography are controlled by PAGE and western blot. Therefore, the samples are prepared according to Table 25.

Table 25: Preparation of PAGE purification check samples.

fraction	24 µL
4x sample buffer	8 µL
Total	32 µL

After mixing, the samples are heated at 98 °C for 10 min and spun down. 10 µL of the samples are loaded on the gel.

4.2.5.5.4 Electrophoresis

The gel is placed in the electrophoresis chamber, which is then filled up with 1x running buffer. The samples and the standard are applied and the electrophoresis is run. The gel is dyed for 10 min in staining solution, washed with d H_2O, and incubated in destaining solution for at least 12 hours. Saturated destaining solution is replaced with fresh one.

4.2.5.6 Western blot

Prepare: 2x SDS gel, TBS, blotting buffer, TBST

The SDS gels and samples are prepared and the electrophoresis is run. It is recommendable to produce two identical gels staining one with Coomassie and using the other for further western blot procedure. The nitrocellulose membrane is wetted with TBS. The blotting clamp is covered with blotting buffer and the sponge-filter paper-gel-membrane-filter paper-sponge sandwich is adjusted in respect to the anode. The clamp is sealed, ensuring an air free assembling, placed in the electrophoresis chamber and an ice block is inserted to ensure cooling during the transfer. The electrophoresis is run at 180 mA for 1 h. Afterwards the membrane is stained reversibly with Ponceau S for 5 min and washed with dd H2O to test the transfer efficiency. The lanes and the dye front are marked with a pencil and then the membrane is washed 3x for 5 min in TBST followed by 1 h of blocking with 7.5 % milk powder solution in TBST at room temperature. Afterwards, the membrane is washed with 1x TBST for 5 min before incubation with anti-his antibody from rabbit (1:2000) in 2.5% milk powder in TBST at 4 °C on a shaker overnight. The next day the membrane is washed 3x with TBST for 10 min before incubation with the HRP-linked anti-rabbit antibody (1:5000) in 2.5% milk powder in TBST for 1 hour. Afterwards, the membrane is washed 3x with TBST for 10 min and 1x with TBS for 5 min. For detection Luminol is mixed with H_2O_2 (both from kit) (1:1, vol:vol) and thoroughly applied on the membrane by pipetting. The signal is visualized on a photo film in the darkroom.

4.2.6 Characterization of the enzymes

4.2.6.1 UV/VIS absorption spectra

To record the UV/VIS absorption spectrum of an enzyme it is diluted in buffer (50 mM Tris, 150 mM NaCl, pH 8) and the spectrum is recorded from 300 – 800 nm. To evaluate the pH dependence of the spectra of the wild type protein, *At*BBE15 is recorded in buffers with pH range from 4–9.

4.2.6.2 Determination of extinction coefficients of variants

To determine the extinction coefficient of a flavoprotein the enzyme was diluted to an absorbance of 0.1 at 450 nm in 50 mM Tris and 150 mM NaCl pH 8 and the spectra were recorded. 100 µL 10% SDS solution was added and the enzyme solution was heated for 30 min at 95°C. Afterwards the spectrum was recorded again.

4.2.6.3 Determination of pH dependent extinction coefficient of DCPIP

To determine the extinction coefficient of DCPIP at different pH values a 2 mM DCPIP stock solution in dd H_2O is prepared. Afterwards 25 µL of the DCPIP stock solution are added to 975 µL of buffer with 50 mM citrate and 150 mM NaCl (pH 5-6) or 50 mM potassium phosphate and 150 mM NaCl (pH 7-7.75) or 50 mM Tris and 150 mM NaCl (pH 8-9) to reach a final concentration of 50 µM. The same buffer is used as reference and the spectrum is recorded from 350 to 800 nm. All samples are prepared and measured in triplicates at 25 °C respectively. The absorbance value at 600 nm is used to calculate the extinction coefficient of DCPIP at 900 nm at the respective pH.

4.2.6.4 Michaelis-Menten kinetics

To probe reactivity of AtBBE-like 15 wild type enzyme towards the substrate cinnamylic alcohol a Michaelis Menten kinetic study was performed to evaluate proper conditions for probing the pH optima of the variants. All ingredients but enzyme are used in the same concentration as reference. A distinct concentration of enzyme is added and thoroughly mixed. The decreasing absorption is recorded for 160 s. All samples are measured in triplicates at 25 °C. The decreasing absorption over time is transformed to decreasing concentration of DC-PIP over time by its extinction coefficient at the respective pH values which are determined with a DC-PIP stock solution

Table 26: Mixture for Michaelis Menten kinetics.

KPi buffer (50 mM, pH 7)	900 µL
Substrate (50-5000 µM)	50 µL
DCPIP (4 mM)	30 µL
AtBBE-like15 (4 µM)	20 µL
Total	1000 µL

4.2.6.5 pH-dependent steady state activity assay

The activity is tested in buffers with, 100 mM potassium phosphate and 150 mM NaCl (pH 6-7.75) or 100 mM Tris and 150 mM NaCl (pH 8-9), a final concentration of **500 µM Cinnamylalkohol** in dd H_2O as substrate and a final concentration of **120 µM DC-PIP** in dd H_2O as electron acceptor. Buffer, substrate and DC-PIP are incubated at 25 °C for 2 min then absorption at 600 nm is recorded for 20 sec. All ingredients but enzyme are used in the same concentration as reference. A distinct concentration of enzyme is added and thoroughly mixed. The decreasing absorption is recorded for 160 s. All samples are measured in triplicates at 25 °C. The decreasing absorption over time is transformed to decreasing concentration of DC-PIP over time by its extinction coefficient at the respective pH values which are determined with a DC-PIP stock solution and are in good agreement with previously published data.

Table 27: Mixture for Michaelis Menten kinetics.

buffer (50 mM pH 5-9)	900 µL
Cinnamyl alcohol (5 mM)	50 µL
DCPIP (4 mM)	30 µL
Enzyme	20 µL
Total	1000 µL

4.2.6.6 Pre steady state activity assay

The activity of each variant is tested at the pH optimum as determined by steady state kinetics in buffers 50 mM potassium phosphate and 150 mM NaCl (pH 7-7.75) or 50 mM Tris and 150 mM NaCl (pH 8-8.5) and final concentrations of the substrates cinnamyl alcohol or coumaryl alcohol ranging from 62.5 µM to 5 mM in buffer corresponding to the pH optimum of the measured variant. All experiments were done in a stopped flow device under oxygen-free atmosphere at 25 °C. Upon addition of enzyme, absorption spectra were recorded until no decrease in absorption at 450 nm is observable. All samples are measured in triplicates. On the decreasing absorption at 450 nm at each substrate concentration, an exponential fit is applied and the resulting kobs is used to determine k_{red} and K_D via a hyperbolic fit using origin.

4.2.7 Computational modeling of a bicovalent linked isoalloxazine ring

The conformation of the isoalloxazine ring are optimized using the GAUSSIAN 09 suite of programs with the RHF (restricted Hartree Fock) (determination of the wave function method with the basis set 6-31++G**). The ribityl-phosphate-nucleotide side chain is modeled by an ethyl group. The attached amino acids are modeled without the backbone. First the stationary point energy of the fully oxidized form is calculated once in gas phase and once in PCM (polarizable continuum model) the latter simulating an aqueous environment. The calculation is visualized with Molden. In a second step the

planar molecules of step 1 are used as a template and the fully reduced form is modeled by adding a hydride to the N5 position of the isoalloxazine ring. Again the energy minimum is calculated as explained above. In a third step the hydride is removed and the calculation is repeated, leading to a planar molecule again. with the basis set 6-31++G** (term for MO with polarisable and diffuse functions) in PCM mode simulating aqueous environment. Once the fully oxidized form is optimized, the addition of a hydride at the N5 position is simulated and a bending of the ring is observed. By removal of the hydride the ring moved back to its planar form again and the Energy difference between these two states is calculated.

4.2.8 Computational modeling of phylogenetic trees

The subdirectories *dist* and *boot-dist* are created. The *M-Coffee* alignment in *PHYLIP* format is pasted and renamed to *infile*. Outtrees have a Newick tree format which is not readable for humans, but the outfile is. The bootstrapped distance method tree is calculated by *seqboot*, *protdist*, *fitch* and *consense* with the parameters indicated in the diagram below. The infiles had to be renamed after each program.

4.2.9 Data processing

All the calculations are carried out with Microsoft Excel 2010, the hyperbolic fits in Michaelis-Menten kinetics and pre steady state kinetics is generated with Origin 7.

4.2.9.1 Spectra

The data are imported from .csv files created from WIN ASPECT software. The blank is assumed as absorption value at 600 nm and is subtracted from the remaining absorption values. The spectra are plotted and normalised accordingly. The protein concentration is calculated at 450 nm with an extinction coefficient of 5960 M^{-1} cm^{-1}.

$$[E] = \frac{A}{\varepsilon_{450} \cdot d} \cdot 10^6$$

[E]…concentration of enzyme [µM]
A…absorption (A_{450})
ε_{450}…extinction coefficient *At*BBE-FAD at 450 nm (5960 $M^{-1} \cdot cm^{-1}$)
d…width of cuvette [cm]

Equation 5: Rewritten Beer-Lambert law to calculate the concentration of the protein sample.

4.2.9.2 Determination of extinction coefficients of the variants

To determine the extinction coefficient of the proteins the spectra was recorded. After heating the samples and addition of SDS the spectra are recorded again and the

4.2.9.3 Determination of extinction coefficients of variants

To determine the extinction coefficient of a flavoprotein Equation 6 was used.

$$\varepsilon_{450,var} = \frac{A_{nat} \cdot \varepsilon_{450,FAD}}{A_{denat}} \cdot v$$

$\varepsilon_{450,var}$...extinction coefficient *At*BBE-FAD at 450 nm [$M^{-1} \cdot cm^{-1}$]
$\varepsilon_{450,FAD}$...extinction coefficient FAD at 450 nm (11300 $M^{-1} \cdot cm^{-1}$
A_{nat}...absorption (A_{450}) of native enzyme
v...dilution factor (1.13)

Equation 6: Calculation of the extinction coefficients of the variant proteins.

4.2.9.4 Determination of pH dependent extinction coefficient of DCPIP

To evaluate the extinction coefficient of DCPIP Equation 7 was used.

$$\varepsilon_{600} = \frac{\Delta A}{c \cdot d} \cdot 10^6$$

ε_{600}...extinction coefficient [$M^{-1} \cdot cm^{-1}$]
ΔA… difference in absorption value of 800 nm and 600 nm []
c…concentration of DCPIP (50 µM)
d…width of cuvette [cm]

Equation 7: Rewritten Beer-Lambert law to calculate the extinction coefficient (ε) of DCPIP at 600 nm at different pH.s

4.2.9.5 Activity assay

The data are imported from .csv files created from WIN ASPECT software. At 0 sec, absorption of 0 is assumed as blank. The absorption is plotted over time in seconds. A linear fit is made and the slope (decreasing absorption per second) is determined.

4.2.9.6 Michaelis-Menten kinetics

The data are imported from .csv files created from WIN ASPECT software. At 0 sec, absorption of 0 is assumed as blank. The absorption is plotted over time in seconds. A linear fit is made and slopes (decreasing absorption per second) are determined. The mean slope and the standard deviation are calculated for the triplicate measurements at each concentration. The initial reaction velocity is calculated according to Equation 8.

$$v = \frac{Abs}{sec} \cdot \frac{1}{\varepsilon_{600} \cdot d}$$

v...rate [$M \cdot s^{-1}$]
Abs/sec...rate of destaining [s^{-1}]
ε_{600}...molar extinction coefficient of DCPIP at 600 nm [$M^{-1} \cdot cm^{-1}$]
d...width of cuvette (1 cm)

Equation 8: The rate for the destaining reaction of DCPIP is calculated for each variant.

4.2.9.7 pH-dependent steady state activity assay

The decreasing absorption over time is transformed to decreasing concentration of DC-PIP over time by its extinction coefficient at the respective pH value which is determined with a DC-PIP stock solution and are in good agreement with previously published data. Kcat is calculated by using equation. The turnover number kcat is calculated according to Equation 9.

$$k_{cat} = \frac{v}{[E]}$$

kcat... turnover number [s^{-1}]
v... rate [$M \cdot s^{-1}$]
[E]...concentration of enzyme [M]

Equation 9: Calculation of the turnover number in steady state approach.

4.2.9.8 Pre steady state activity assay

On the decreasing absorption at 450 nm at each substrate concentration, an exponential fit is applied and the resulting k_{obs} are used to determine k_{red} and K_D via a hyperbolic fit using origin.

5 Results

5.1 *At*BBE-like 15 - site directed mutagenesis study of the active site

In the course of the studies of the catalytic mechanism of *At*BBE-like 15 the spectral properties of the wild type protein and its active site variants were analyzed and their extinction coefficients were calculated based on the absorption of the denatured protein. Further, a study on the pH optima of the activity toward cinnamyl alcohol with DCPIP as final electron acceptor was performed. Therefore, the extinction coefficient of DCPIP at 600 nm was determined for each pH tested. To ensure proper setting for the activity assay the saturating substrate concentration was evaluated by Michaelis Menten kinetics. With the determined extinction coefficient of the enzymes the apparent turnover number k_{cat} were calculated. The wild type proteins as well as two variants (R292M and Q438V) were also tested on coumaryl alcohol under pre steady state conditions in the stopped flow at their respective pH optimum. R292M was additionally probed on cinnamyl alcohol.

5.2 UV/VIS absorption spectra

To gain information on the mode of cofactor binding and to determine the concentration of the active enzyme portion via Beer-Lambert law, UV/VIS absorption spectra were recorded. In Figure 6 the resulting spectra of *At*BBE-like 15 wild type enzyme and the variants are depicted in the overall view (A and B) and in detail (C and D). The observed local maxima of the spectra shown in Figure 6 are listed in Table 28.

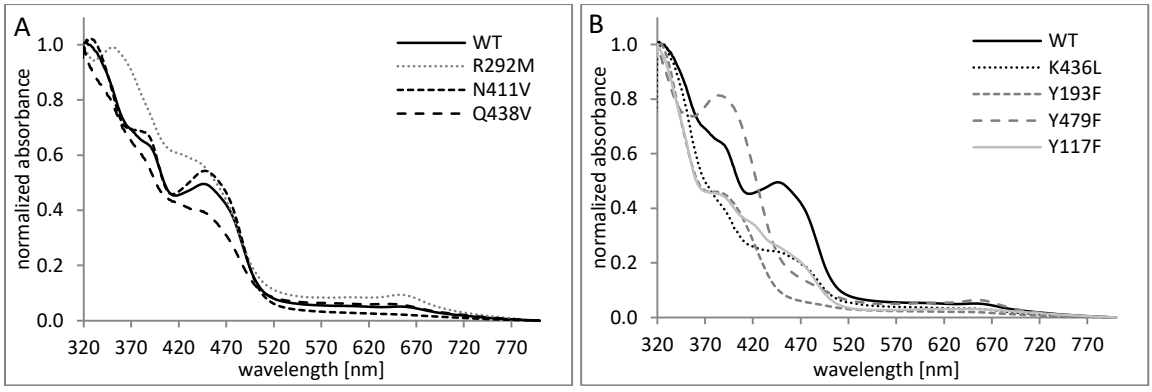

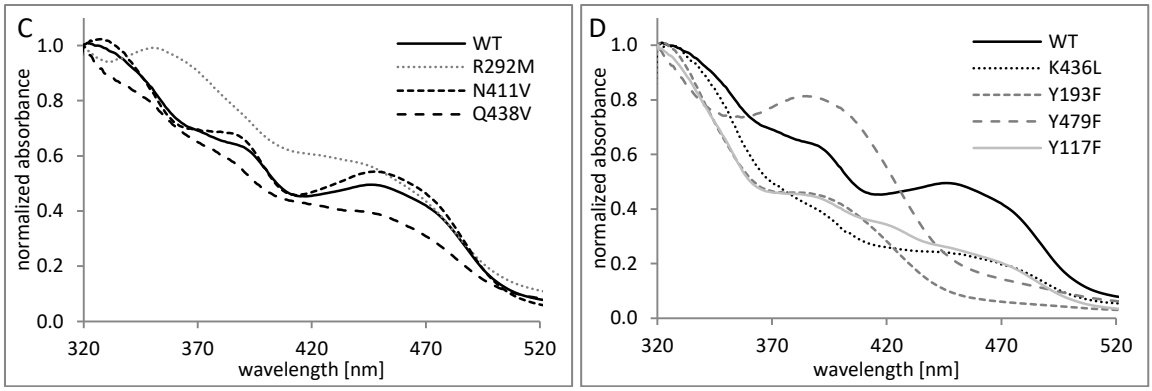

Figure 6: UV/VIS were performed absorption spectra of *At*BBE-like 15 wild type (WT) and the active site variants normalized to 320 nm. The spectra were recorded in 50 mM Tris, 150 mM NaCl pH 8. In the upper row the overall spectra are depicted. In the bottom row the spectral properties of the flavin are depicted in detail. In **panel A and C** the absorption spectra of the WT and the variants R292M, N411V and Q438V are depicted. In **panel B and D** the absorption spectra of the WT and the variants K436L, Y193F, Y479F and Y117F are depicted.

Table 28: Local absorption maxima observed in the UV/VIS spectra of *At*BBE-like 15 wild type protein and the produced active site variants recorded in 50 mM Tris, 150 mM NaCl at pH 8.

Variant	λ_{max} 1 [nm]	λ_{max} 2 [nm]	λ_{max} 3 [nm]	λ_{max} 3 [nm]
WT	367	383	-	445
R292M	350	-	-	437
N411V	-	380	-	445
Q438V	-	380	418	446
K436V	-	380	-	446
Y193F	-	383	-	-
Y479F	-	383	-	-
Y117F	-	385	418	446

The UV/VIS absorption spectrum of **wild type** *At*BBE-like 15 revealed two characteristic but weakly pronounced peaks resulting from the bicovalently linked FAD. The properties of the **R292M** variant in the UV/VIS absorption spectrum reveal an unusual hypsochromic shift of the peak at 380 nm to 350 nm. Also the peak at around 445 nm is blue shifted to approximately 437 nm. Comparing the spectra of the denatured and the native variant, it is apparent that the absorption maximum at approximately 440 nm is more similar compared to any other variant. The spectral properties of the **Q438V** variant in the UV/VIS absorption spectrum show similarities to the wild type spectrum but both peaks are weakly pronounced. Also a tiny shoulder is detected at approximately 420 nm, which is not expected for a usual flavin spectrum. This effect is even more pronounced in the Y117F variant lacking the hydroxyl group of the tyrosine residue. The **N411V** UV/VIS absorption spectrum is similar to the wild type spectrum but the peaks at approximately 380 nm and 450 nm are more pronounced. The absorption spectrum of the **K436L** variant shows similarity in shape to the spectrum of the wild type but both peaks at 380 nm and 445 nm are not pronounced. The extinction coefficient for this variant was determined to 3 000 $M^{-1} \cdot cm^{-1}$ and therefore 60% of the extinction coefficient of the wild

type protein. The absorption spectra of the **Y117F** variant shows a peak at 385 nm similar to the wild type but gives rise to a peak at 418 nm also slightly observed in the Q438V variant. A strong loss of intensity of the 450 nm peak was also detected. The absorption spectrum of **Y193F** variant reveals a strongly pronounced broad peak at 380 nm and no observable peak at 450 nm representing the catalytic active enzyme. This effect is also detected and but weaker pronounced in **Y479F**. The spectrum is unusual for a flavoprotein since the peak at 450 nm representing the active portion of enzyme is not present, at all.

To evaluate the influence of pH on the spectral properties of the enzyme the absorption spectra of the *At*BBE-like 15 were recorded in a range from pH 4 to pH 9. The result is depicted in Figure 7.

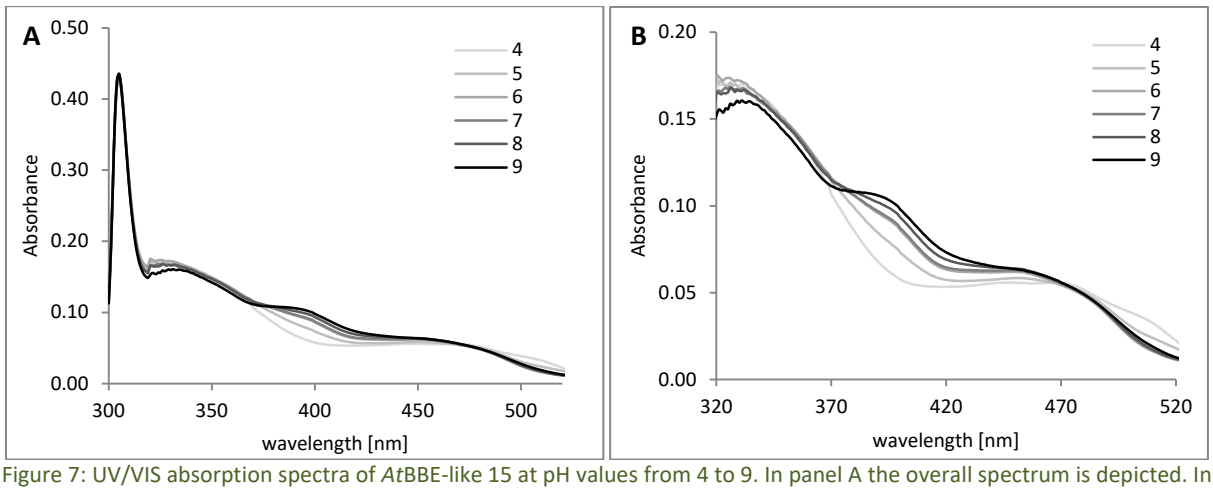

Figure 7: UV/VIS absorption spectra of *At*BBE-like 15 at pH values from 4 to 9. In panel A the overall spectrum is depicted. In panel B the absorbance of the flavin is depicted in detail. The measurements were performed in 50 mM citrate, phosphate or Tris buffer and 150 mM NaCl.

In Figure 7 the UV/VIS absorption spectrum of *At*BBE-like 15 at various pH is depicted (looks as it is red shifted for 7 nm corrected by hand). The peak at 380 nm seems to be strongly affected by the changes in pH. At pH 6-7 the peak becomes visible and gets more pronounced in a more basic environment. At pH 5 and lower the peak is not visible and the protein gives rise to a high absorption at 500 nm.

5.3 Determination of extinction coefficients of the variants

To calculate the extinction coefficient and to evaluate the cofactor tethering of *At*BBE-like 15 and the active site variants the absorption spectra of the denatured enzymes were recorded and are depicted in Figure 8. The observed local maxima of the UV/VIS absorption spectrum of denatured *At*BBE-like 15 and the active site variants are listed In Table 29. From the absorption value of the native and the denatured proteins at 450 nm, the extinction coefficients of the flavoenzymes were determined

using Equation 6 and the molar extinction coefficient of free FAD 11,300 $M^{-1} \cdot cm^{-1}$. The results are listed in Table 30.

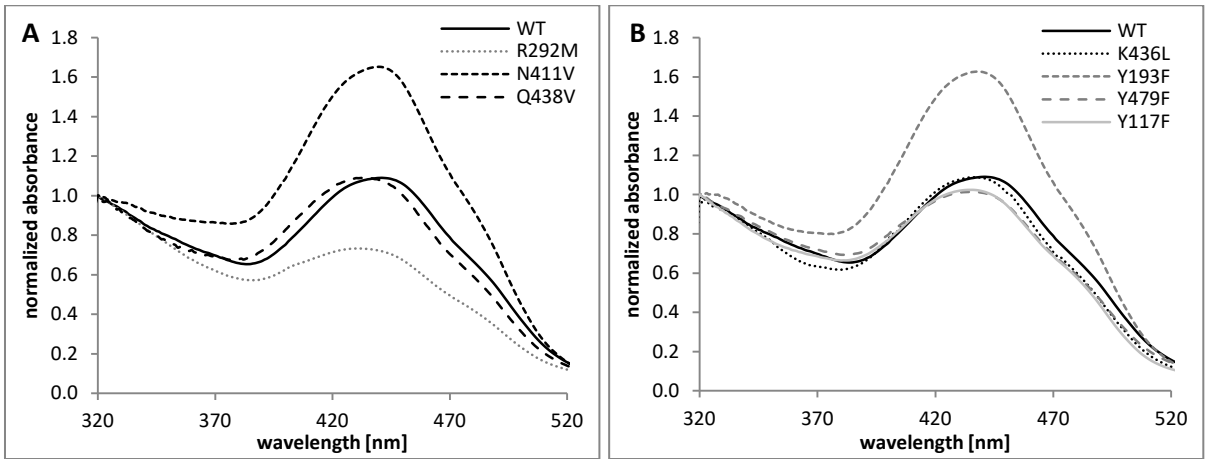

Figure 8: UV/VIS absorption spectra of denatured *At*BBE-like 15 wild type protein (WT) and the active site variants normalized to 320 nm. The spectra were recorded in 50 mM Tris, 150 mM NaCl and 2.3% SDS at pH 8. In panel A the absorption spectra of the denatured wild type protein (WT) and the variants R292M, N411V, and Q438V are depicted. In panel B the absorption spectra of the denatured wild type protein (WT) and the variants K436L, Y193F, Y479F and Y117F are shown.

Table 29: Results of the UV/VIS spectral scan of denatured *At*BBE-like 15 and the active site variants. The local absorption maxima are listed with

	WT	N411V	K436V	Q438V	Y117F	R292M	Y193F	Y479F
λ_{max} [nm]	441	439	435	433	436	433	439	437
Δ WT	-	-2	-6	-8	-5	-8	-2	-4
Δ 445 nm (8α-N-His) [42]	-4	-6	-10	-12	-9	-12	-6	-8
Δ 437 nm (6-*S*-Cys) [42]	+4	+2	-2	-4	-1	-4	+2	0

The absorption maximum in the absorption spectrum of the denatured wild type enzyme was determined with approximately 441 nm. This is in good accordance to the findings of Winkler *et al*. in the *Ec*BBE [8] and other enzymes harbouring bicovalently attached FAD cofactors. The variants all exhibit a single peak in their spectra but their absorption maxima are blue shifted upon denaturation ranging from -2 nm for N411V and Y193 to -8 nm for Q438V and R292M.

Table 30: Results of the calculation on the extinction coefficients of *At*BBE-like 15 and the active site variants. The absorbance (A) at 450 nm and the extinction coefficient of free FAD 11300 $M^{-1} \cdot cm^{-1}$ was used in Equation 6.

variant	A_{nat}	A_{denat}	c_{denat} [µM]	c_{nat} [µM]	ϵ_{450} [$M^{-1} \cdot cm^{-1}$]	rel. ϵ_{450}
WT	0.1981	0.4058	36	41	**4900**	100%
R292M	0,1962	0,1997	18	20	**9800**	200%
N411V	0.1246	0.3030	27	30	**4100**	84%
Q438V	0.0804	0.1526	14	15	**5300**	108%
K436V	0.0890	0.2950	26	29	**3000**	61%
Y193F	0,0333	0,3855	34	38	**900**	18%
Y479F	0,0541	0,2184	19	22	**2500**	51%
Y117F	0,1088	0,3409	30	34	**3200**	65%

The extinction coefficient of R292M was determined with 9 800 $M^{-1} \cdot cm^{-1}$. It is therefore 200% of the wild type extinction coefficient and the highest determined in the variants. If the extinction coefficient was overestimated the concentration is underestimated following Lambert-Beer law. The extinction coefficient for Y193F was determined with 900 $M^{-1} \cdot cm^{-1}$ and is therefore only approximately 20% compared to the extinction coefficient of the wild type enzyme. Also it is the lowest extinction coefficient detected in the variants. If the extinction coefficients were underestimated the concentration of the enzyme is overestimated according the Lambert-Beer equation.

5.4 pH optima in steady state kinetics

To evaluate the pH optima of *At*BBE-like 15 and the produced active site variants under steady state conditions a DCPIP based assay was performed and 500 µM cinnamyl alcohol was used as substrate as determined before in Michaelis-Menten approach. The resulting graphs of the measurement are depicted in Figure 10 Figure 11 and and are summarized in Table 31 and Figure 12. With the determined extinction coefficients a turnover number was estimated for each enzyme and the results are listed in Table 32 and are depicted in Figure 13.

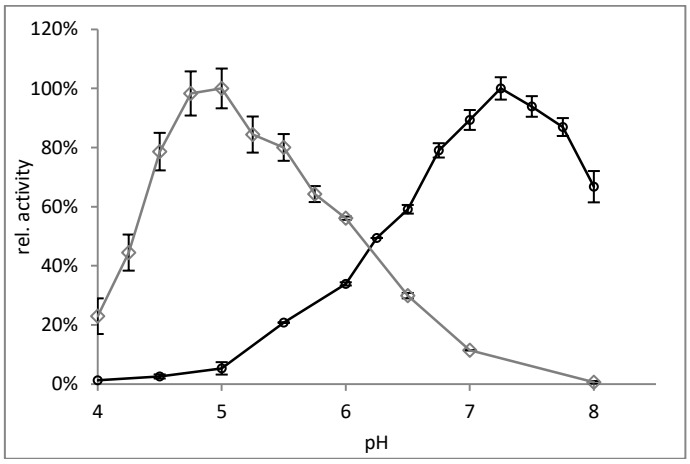

Figure 9: pH optima determined in DCPIP activity assay with 500 µM cinnamyl alcohol (black) or 1000 µM coniferyl alcohol (grey) under steady state conditions of *At*BBE-like 15. The measurements were performed in 50 mM KPi or Tris and 150 mM NaCl.

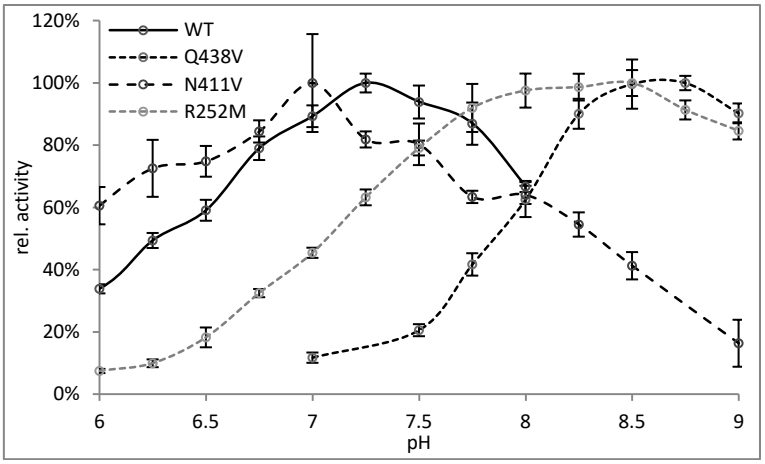

Figure 10: pH optima determined in DCPIP activity assay with 500 µM cinnamyl alcohol under steady state conditions of *At*BBE-like 15 and the active site variants. The measurements were performed in 50 mM KPi or Tris, 150 mM NaCl. Wild type protein (black) and the variants Q438V, N411V and R292M are depicted.

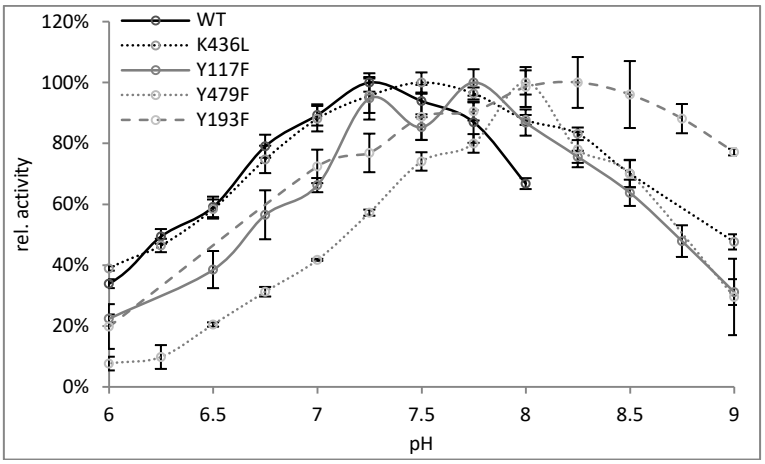

Figure 11: pH optima determined in DCPIP activity assay with 500 µM cinnamyl alcohol under steady state conditions of *At*BBE-like 15 and the active site variants. The measurements were performed in 50 mM KPi or TRIS/HCl and 150 mM NaCl. Wild type protein and the variants K436L, Y117F, Y479F and Y193F are depicted.

Table 31: Overview of the determined pK_a values and pH optima in DCPIP activity assay with 500 µM cinnamyl alcohol under steady state conditions of *At*BBE-like 15 and the active site variants. The pK_a values were estimated as the pH value at 50% activity respectively.

variant	pH_{opt}	ΔpH WT	pK_{a1}	pK_{a2}
WT	7.3	-	6.3	8.3*
N411V	7.0	-0.3	<6	8.3
K436L	7.5	+0.2	6.3	9.0
Y117F	7.8	+0.5	6.5	8.8
Y479F	8.0	+0.7	7.0	8.8
Y193F	8.5	+1.2	6.5	>9*
R292M	8.5	+1.2	7.0	>9*
Q438V	8.5/8.8	+1.5	7.8	>9*

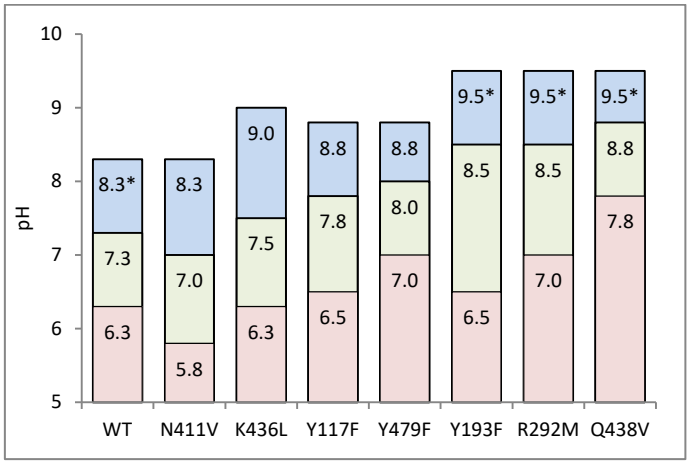

Figure 12: Overview of the determined pK_{a1} values (bottom, red), pH optima (middle, green) and pK_{a2} values (top, blue) in ascending order of the respective pH optimum. The values were estimated from the activity in steady-state assay with 500 µM cinnamyl alcohol as substrate and DCPIP as final electron acceptor. *out of pH range of measurement

pH optima and pK_a-values (Figure 10, Figure 11)

When the activity of *At*BBE-like 15 wild type enzyme towards cinnamyl alcohol in steady state assay with DCPIP as final electron acceptor was tested a pH optimum of 7.3 was found. The enzyme preserves 80% of its activity in the range of 0.8 pH units (7.0-7.8). The estimated inflection points of the relative activity graph at 50% are 6.3 and 8.3 (out of range). The shape of the pH optimum graph indicating a sharp maximum and two minor shoulders at pH 7 and pH 7.8. The pH optimum determined for **R292M** is 8.5 and therefore +1.2 pH units higher than the wild type pH optimum. Together with Y193F, Y479F and Q438V this variant exhibit the highest shift in the optimum. It preserves 80% of its activity in the range of 1.2 pH units (7.8-9) similar to Y193. The shape of the pH optimum graph is broad and no sharp optimum is visible (similar shape than in the Y193F variant). The estimated inflection point of the relative activity graph at 50% and therefore the pK_a values are 7.0 (same as for Y479F, +0.7 compared to WT) and higher than 9.0 (also determined for Y193 and probably Q438). The pH optimum determined for **Q438V** is 8.5-8.8 and therefore +1.5 pH units higher than the wild type optimum. Together with Y193F, Y479F and R292M this variant depicted the highest shift in the optimum. It preserves 80% of its activity in the range of 0.7 pH units (8.3-9.0). The shape of the pH optimum graph is narrow and smooth. The estimated inflection point of the relative activity graph at 50% and therefore the pK_a values are 7.8 (+1.5 compared to WT) and higher than 9.0 (also determined for Y193F and R292M). The pH optimum determined for **N411V** is 7.0 and therefore -0.3 pH units lower than the wild type optimum and the lowest optima detected in the variants. It preserves 80% of its activity in the range of 0.7 pH units (6.8-7.5). The shape of the pH optimum graph indicating a sharp maximum and two shoulders at pH 6.3 and pH 7.5. The estimated inflection point of the relative activity graph at 50% and therefore the pK_a values are at 5.8 (-0.5 compared to

the WT) and 8.3 (same as approx WT). The pH optimum determined for **K436L** is 7.5 and therefore +0.2 pH units higher than the wild type optimum. It preserves 80% of its activity in the range of 1.3 pH units (7.0-8.3) resulting in a broad flat peak appearance also detected in R292M and Y193F. The estimated inflection point of the relative activity graph at 50% and therefore the pK_a values are estimated at 6.3 (same as WT) and 9.0 (pK_{a2} 8.8 determined for Y117 and Y479F and approx +0.3 of WT). The pH optimum determined for **Y117F** is 7.8 and therefore +0.5 pH units higher than the wild type enzyme. It preserves 80% of its activity in the range of 0.8 pH units (7.3-8.0). The shape of the pH optimum graph indicating two optima at 7.3 and 7.8. The estimated inflection point of the relative activity graph at 50% is 6.8 (same as determined for Y193F, +0.5 compared to WT) and 8.6 (also determined for K436L and Y479F, approx +0.3 of WT). The pH optimum determined for **Y193F** is 8.5 and therefore +1.2 pH units above the wild type optimum. Together with R292M, Y479F and Q438V this variant depicted the highest shift in the optimum. It preserves 80% of its activity in the range of 1.2 pH units (7.5-8.8) and therefore reveals together with R292M and K436L the broadest optimum. The shape of the pH optimum graph does not depict a sharp optimum (similar shape than R292M). The estimated inflection point of the relative activity graph at 50% is 6.5 (also determined for Y117F, +0.5 compared to WT) and higher than 9.0 (also determined for R292M and probably Q438). The pH optima of **Y479F** was determined with 8.0 and therefore +0.7 pH units above the wild type optimum. Together with R292M, Y193F and Q438V this variant depicted the highest shift in the optimum. It preserves 80% of its activity in the range of 0.2 pH units (7.8-8.0). The shape of the pH optimum graph indicating a sharp maximum with two shoulders at pH 7.5 and pH 8.5. The estimated inflection point of the relative activity graph at 50% is 7.0 (same as for R292M) and 8.8 (also determined for K436L (9.0) and Y117F).

Table 32: Overview of the k_{cat} values and relative k_{cat} values in respect to the wild type enzyme at pH optimum determined under steady state conditions in DCPIP-assay with 500 µM cinnamyl alcohol as substrate. The max rate was calculated with the extinction coefficient determined for DCPIP at the respective pH optimum. The concentration of active enzyme was estimated by the absorbance at 450 nm and the extinction coefficient ε_{450} of the variant or WT enzyme, respectively. *The extinction coefficient for the wild type enzyme was determined by Bastian Daniel in his dissertation.

	pH_{opt}	rate $[M \cdot s^{-1}]$	c_{enzym} [nM]	ε_{450} $[M^{-1} \cdot cm^{-1}]$	k_{cat}, $\varepsilon_{450,var}$ $[s^{-1}]$	k_{cat}, $\varepsilon_{450,WT}$ $[s^{-1}]$	rel. k_{cat} $\varepsilon_{450,var}$	rel. k_{cat} $\varepsilon_{450,WT}$
WT	7.3	$4.8 \cdot 10^{-8}$	150	4960*	0.32 ± 0.01	0.32 ± 0.01	100%	100%
Y479F	8.0	$7.8 \cdot 10^{-8}$	400	2500	0.20 ± 0.01	0.10 ± 0.00	61%	31%
Y117F	7.8	$5.9 \cdot 10^{-8}$	440	3200	0.17 ± 0.01	0.11 ± 0.01	52%	33%
N411V	7.0	$1.7 \cdot 10^{-8}$	175	4100	0.10 ± 0.02	0.08 ± 0.01	30%	25%
K436V	7.5	$4.6 \cdot 10^{-8}$	470	3000	0.10 ± 0.00	0.06 ± 0.00	30%	18%
R292M	8.5	$6.1 \cdot 10^{-8}$	800	9800	0.08 ± 0.00	0.15 ± 0.01	24%	47%
Q438V	8.8	$3.0 \cdot 10^{-8}$	2000	5300	0.01 ± 0.00	0.01 ± 0.00	4%	4%
Y193F	8.5	$8.2 \cdot 10^{-9}$	800	900	0.01 ± 0.00	<0.01	3%	1%

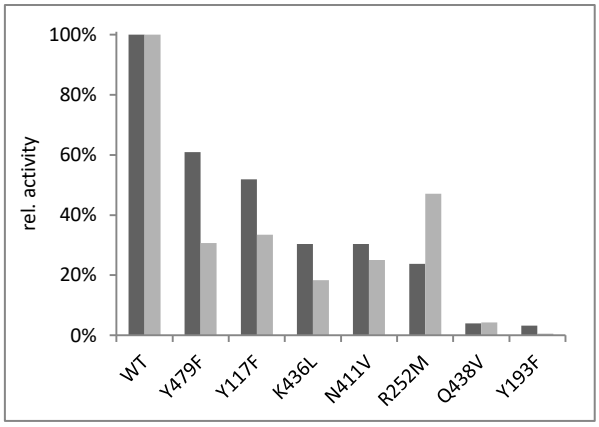

Figure 13: Graphical representation of the calculated relative k_{cat} values evaluated by DCPIP activity assay with 500 µM cinnamyl alcohol under steady state conditions at the respect pH optimum. The k_{cat} calculated with the enzyme concentration determined with the variants extinction coefficient respectively is represented by the dark bar. The k_{cat} calculated with the enzyme concentration determined with the wild type enzymes extinction coefficient are represented by the light gray bar. In panel A the variants are in descending order in respect to their relative k_{cat} determined with the extinction coefficient of the variant In panel B the variants are in descending order in respect to their relative k_{cat} determined with the extinction coefficient of the wild type enzyme.

Turnover numbers

Based on the extinction coefficient of approximately 4960 $M^{-1} \cdot cm^{-1}$ a turnover number of 0.32 s^{-1} was estimated for the wild type enzyme in steady state approach. The estimated turnover number for the R292M variant is 0.08 s^{-1} and therefore approximately 25% compared to the wild type enzyme. Taking the spectral properties of the variant in account it is possible that the determined extinction coefficient of the variant is overestimated and the turnover number is therefore underestimated. The calculation with the extinction coefficient of the wild type enzyme results in a catalytic activity of 50% compared to the wild type enzyme. The estimated turnover number for the **Q483V** variant is 0.01 s^{-1} and therefore only 4% compared to the wild type (same with both extinction coefficients). Together with Y193F this is the greatest loss in activity found for the variants. The estimated turnover number for the **N411V** variant is 0.10 s^{-1} and therefore approximately 30% compared to the wild type enzyme and a comparable loss of activity with R292M and K436L. Calculations on the turnover number of **K436L** with the extinction coefficient determined for the wild type enzyme resulted in catalytic activity of 18% compared to the wild type enzyme. The estimated turnover number for the **Y117F** variant is 0.17 s^{-1} and therefore approximately 50% compared to the wild type enzyme and therefore comparable loss of activity with Y479F. The estimated turnover number for the **Y193F** variant is 0.01 s^{-1} and therefore approximately 3% relative of the activity to the wild type enzyme. Together with Q438V this is the greatest loss in activity found in the variants. The estimated turnover number for the **Y479F** variant is 0.20 and therefore approximately 60% compared to the wild type enzyme and therefore comparable loss of activity with Y117F. Calculations on the turnover number with the extinction coefficient determined for the wild type resulted in a catalytic activity of 30%

compared to the wild type enzyme. It is reasonable that the determined extinction coefficient of the variant is underestimated and the turnover number is therefore overestimated.

5.5 Pre steady state kinetics

To evaluate the activity of *At*BBE-like 15, R292M and Q438V at their respective pH optimum under pre-steady state conditions the proteins were mixed with varying amounts of *p*-coumaryl alcohol in a stopped flow device. The results obtained from this analysis are summarized in Figure 14.

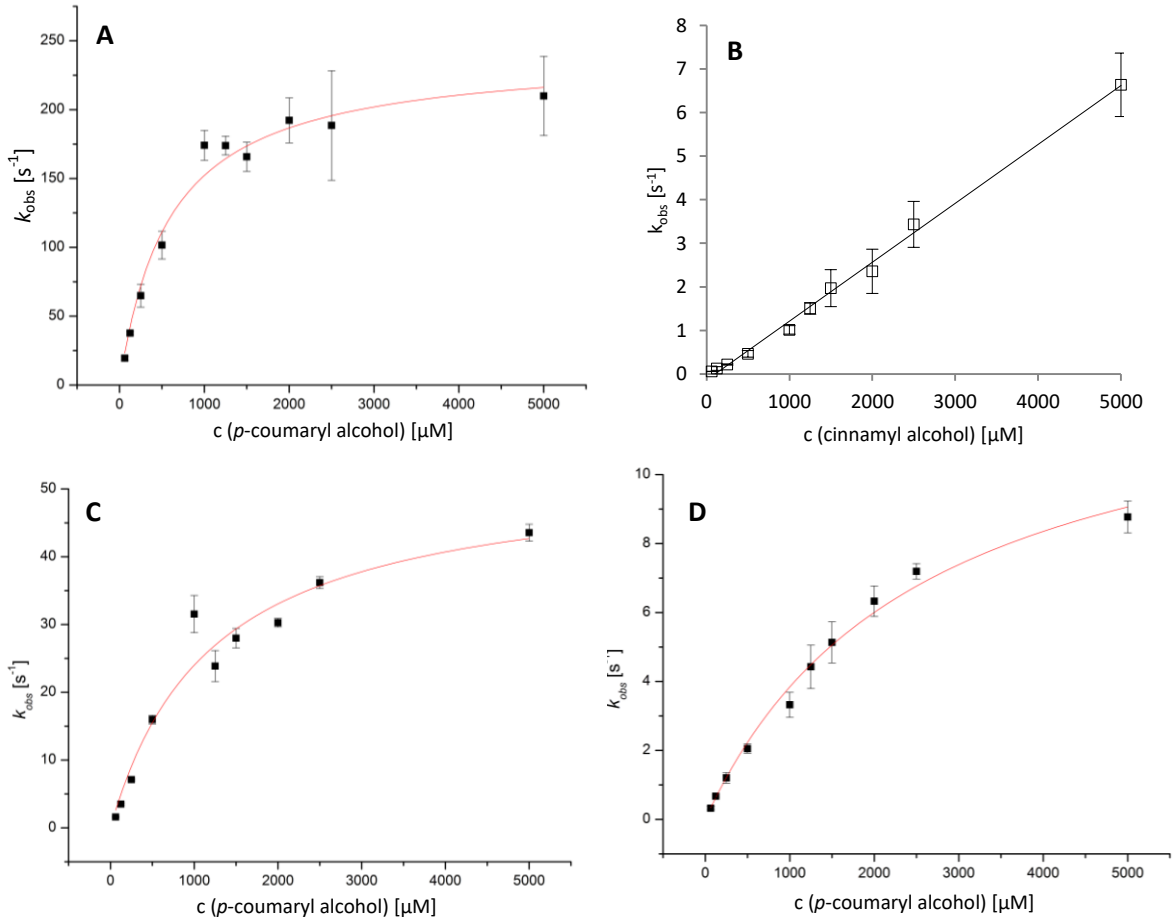

Figure 14: Results of the determined k_{red} in pre steady state approach measured in the stopped flow device at the respective pH optimum. . The enzyme concentration was adjusted to an absorbance of 0.1 at 450 nm and the decrease of the absorption was followed upon reduction and a sigmoid fit was applied giving a certain k_{obs} for each substrate concentration. In panel A the hyperbolic fit for the observed k_{obs} values of the wild type *At*BBE-like 15 with coumaryl alcohol as substrate is depicted. In panel C and D the hyperbolic fit for the observed k_{obs} values of the variants R292M and Q438V with coumaryl alcohol as substrate are depicted respectively. In panel B the linear fit for the observed k_{obs} values of the variants R292M are depicted with cinnamyl alcohol as substrate.

Table 33: Stopped flow results with coumaryl alcohol as substrate at pH optimum and with cinnamyl alcohol as substrate for the R292M variant. Kred and KD was determined by a hyperbolic fit of the observed kobs at different coumaryl alcohol concentrations. Kobs for the R292M variant is estimated at 500 µM cinnamyl alcohol.

	p-coumaryl alcohol				cinnamyl alcohol
variant	k_{red} [s^{-1}]	rel. k_{red}	$K_{D\,e}$[µM]	rel. K_D	K_{obs} [s^{-1}]
WT	241 ± 14	100%	586 ± 115	100%	-
R292M	53 ± 4	22%	1209 ± 238	206%	0.5 ± 01
Q438V	14 ± 1	6%	2572 ± 397	439%	-

For the **wild type enzyme** a reduction rate (k_{red}) at the pH optimum with coumaryl alcohol of 241 s^{-1} and a dissociation constant (K_D) of 586 µM were obtained, which is in good agreement with the results reported by Daniel *et al.* [27]. For the **R292M** variant a k_{red} of 53 s^{-1} was determined which is approximately 20% compared to the wild type enzyme. The estimated K_D value for the variant is approximately two times higher than for the K_D determined for the wild type. For the **Q438V** variant a k_{red} of only 6% compared to the wild type was calculated whereas the K_D value increased more than 4-fold. In pre steady state experiments with the substrate cinnamyl alcohol the reduction rate linearly increased with the substrate concentration and idi no reach a limiting tate up to 5 mM. The k_{obs} for the R292M variant estimated at a substrate concentration of 500 µM cinnamyl alcohol is 0.5 s^{-1} and is therefore 20% compared to the wild type enzyme as determined by Daniel *et al.* [27].

5.6 Determination of pH dependent extinction coefficient of DCPIP

The absorption of 50 µM DCPIP was recorded to determine its extinction coefficient at 600 nm ε_{600} at different pH values. Spectra were recorded at each pH in triplicate at 25°C. To evaluate the quality of the determined extinction coefficient the absorbance at 600 nm was used to calculate the resulting pK_a value of DCPIP which is reflected by the intersection of the linear fit of the plotted logarithmic results.

Table 34: Results of the determined extinction coefficient of DCPIP at 600 nm at various pH. Mean (n=3) Results of the calculation for the determination of the pK_a value of DCPIP.

pH	ε_{600} [$M^{-1} \cdot cm^{-1}$]	pH	$A_{600mean}$	$A-A_{pH5}$	$A_{pH9}-A$	$\log((A-A_{pH5})/(A_{pH9}-A))$
5.0	**5450 ± 120**	5.0	0.2727	0.0000	0.6411	-
5.5	**9000 ± 50**	5.5	0.4708	0.1982	0.4429	**-0.3**
6.0	**13000 ± 50**	6.0	0.6577	0.3850	0.2561	**0.2**
6.3	**14380 ± 70**	6.3	0.7190	0.4464	0.1947	**0.4**
6.5	**15560 ± 50**	6.5	0.7778	0.5052	0.1359	**0.6**
6.8	**16520 ± 120**	6.8	0.8258	0.5532	0.0879	**0.8**
7.0	**16930 ± 100**	7.0	0.8466	0.5739	0.0671	**0.9**
7.3	**17500 ± 40**	7.3	0.8748	0.6021	0.0389	**1.2**
7.5	**17690 ± 40**	7.5	0.8843	0.6116	0.0294	**1.3**
7.8	**17770 ± 40**	7.8	0.8887	0.6160	0.0250	**1.4**
8.0	**17910 ± 80**	8.0	0.8956	0.6230	0.0181	**1.5**
8.3	**18090 ± 30**	8.3	0.9044	0.6317	0.0093	**1.8**
8.5	**18160 ± 90**	8.5	0.9079	0.6352	0.0058	**2.0**
8.8	**18220 ± 90**	8.8	0.9110	0.6383	0.0027	**2.4**
9.0	**18280 ± 190**	9.0	0.9137	0.6411	0.0000	-

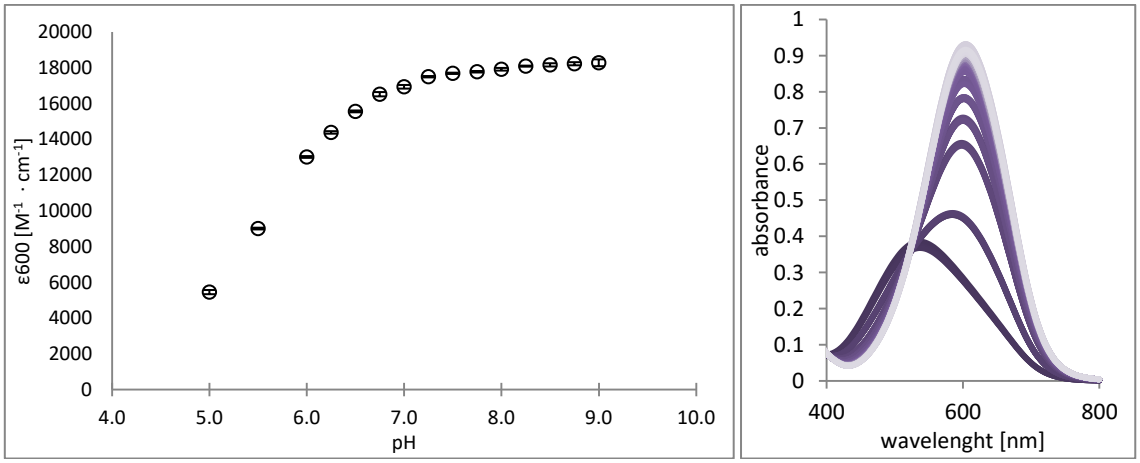

Figure 15: Results of the calculation on the extinction coefficient of DCPIP at 600 nm at various pH. The VIS absorbance measurements were performed in 50 mM Tris, 150 mM NaCl, pH 8 and 25°C in triplicate. On the right the absorbance spectrum of the DCPIP solution at various pH is depicted.

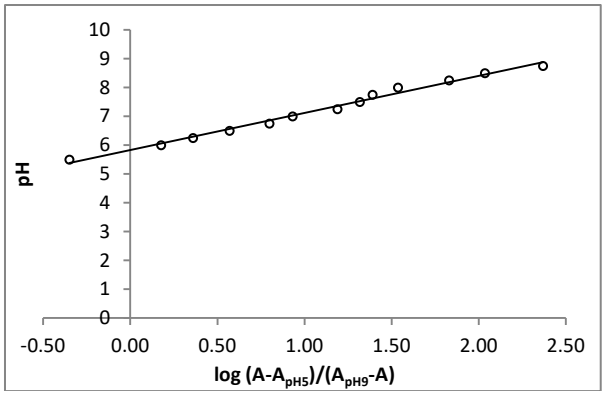

Figure 16: Plotted results of the quality control of the determined extinction coefficients at 600 nm of DCPIP at different pH calculated by EQUATION. The equation resulting from linear fit of the logarithmic absorbance at 600 nm in dependence of the pH giving the pK_a value of DCPIP at the intersection at the y-axis.

The quality control of the determined extinction coefficient at 600 nm for DCPIP at different pH is depicted in Figure 16. The pK_a value of DCPIP was estimated by the measurement of the VIS absorbance and is reflected by the intersection of the linear fit of the logarithmic absorbance values by 5.8. This result is in good accordance to the published value. In this publication from the year 1964 it is also stated that a measurement at the isosbestic point at approximately 520 nm is a reliable method and should be taken in account [43].

5.7 Michaelis Menten kinetics

To determine turnover numbers at various substrate concentrations under steady state conditions the Michaelis-Menten approach was used. The calculated k_{cat} values (Equation 9) are listed in Table 35. The apparent v_{max} is ~0.75 s^{-1} and therefore the apparent K_M value is ~500 µM.

Table 35 Results of the calculated k_{cat} values of *At*BBE-like 15 at various substrate concentrations determined in Michaelis-Menten approach with approximately 80 nM enzyme.

$c_{substrate}$ [µM]	k_{cat} [s^{-1}]
50	0.05 ± 0.04
100	0.09 ± 0.02
200	0.17 ± 0.09
500	**0.32 ± 0.11**
1000	0.54 ± 0.17
2000	0.76 ± 0.18
5000	0.72 ± 0.07

5.8 Computational modeling of bicovalent linked flavins

The results of the calculations of the flavin bending with and without attached amino acids are listed in Table 36 while FAD is the isoalloxazine ring with no amino acids attached, FADHC represents the Cys/His bi-covalent bound isoalloxazine ring. The ribityl-phosphate-

nucleotide side chain was modeled by an ethyl group. The energy difference in the modeled rings is approximately 160 kJ · mol^{-1}. This value corresponds to a number of approximately 9 to 10 hydrogen bonds. This findings lead to the assumption that the enzyme manages to apply force on the isoalloxazine ring to bend it and therefore facilitate the reduction by hydride transfer.

Table 36: Results on the calculation of the bending of the planar flavin reveals a difference in energy and the corresponding number of hydrogen bonds needed.

	E [kJ · mol^{-1}]	No. of hydrogen bonds (17 kJ · mol^{-1})
FAD	153	9.0
FADHC	160	9.4

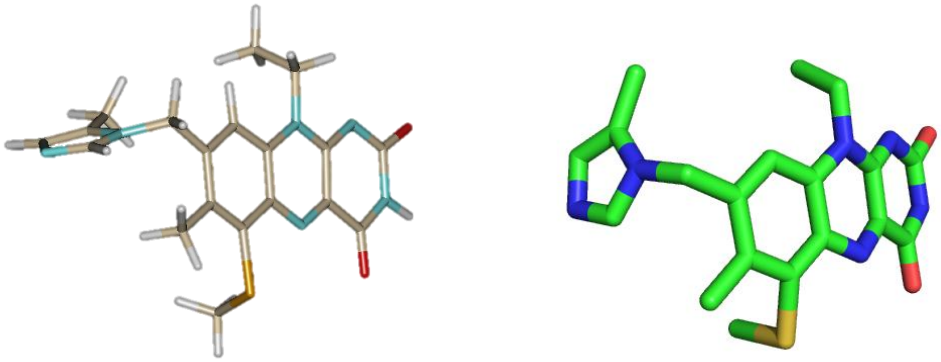

Figure 17: Structures of the bicovalent FAD. On the left the modelled isoalloxazine ring, on the right the isoalloxazine ring elucidated from crystal structure (pdb 4ud8).

6 Discussion

6.1 UV/Vis absorption spectra and extinction coefficients

The evaluation of the UV/VIS absorption spectra of the *K. phaffii* produced enzymes (Figure 6) reveals that a small peak is appearing at around 650 nm which cannot be assigned to the BBE-like proteins but was also detected by Toplak *et al*. [26]. It is presumed to be an impurity since the peak intensity can be decreased by sufficient purification not only by affinity chromatography but also by anion exchange chromatography.

The absorption properties observed in the UV/VIS absorption spectrum of *At*BBE-like 15 were also found for other enzymes harbouring a bicovalent FAD [6], [26]. In contrast to former observations, the absorption around 320-350 nm is usually high in our measurements. Results like this were usually only observed in reduced flavins, as it was found in anaerobic reduction experiments with *Ec*BBE and *Pp*BBE1 or in denatured enzyme [6], [26]. It was also shown that the spectral properties of the FAD

cofactor are not only dependent on its tethering but are also on the pH. As shown before, the oxidized (peaks at 380 and 450 nm) and reduced FAD (peaks at 350 and 400 nm) as well as in the oxidized anionic (peaks at 350 and 450 nm) and the reduced anionic form (peaks at 290 and 350 nm) have different spectral properties [44]. Moreover the mechanism of the cysteinylation of a flavin cofactor is anticipated to be pH dependent needing a base (deprotonated residue) for deprotonating the sulphur of the cysteine prior to the nucleophilic attack at the C6 of the isoalloxazine ring. Also the histidinylation is depending on the pH needing a base for abstracting the proton at the methyl group of the isoalloxazine ring prior to the nucleophilic attack of a nitrogen of the histidine on the 8α-methyl group. In both cases the tethering is achieved by a redox reaction leaving the flavin in a reduced state [2]. The UV/VIS absorption spectrum of *At*BBE-like 15 at various pH depicted in Figure 7 reveals that the peak at 380 nm is affected by the changes of the pH. At pH 6-7 the peak is arising, increasing to pH 9. At pH 5 and lower the peak is not visible and the protein gives rise to a higher absorption at 500 nm. This loss of absorbance at 380 nm was detected upon denaturation in *Ec*BBE with bicovalent or 6-*S*-cystenyl bound FAD [6].

The variant **R292M** has an unusual flavin absorption spectrum with a prominent peak at 350 nm and a blue shifted 450 nm peak comparable with the peak present in the spectrum of the denatured enzyme or of mono-covalent cysteinylated FAD. Nevertheless the peaks in the spectrum of R292M are very well pronounced but not sharply distinguished. It seems that the state of the bicovalent FAD is influenced in this variant giving rise to a mixture of cysteinylated and histidinylated FAD. It is also questionable if this impairing of cofactor binding is stronger effected by a change in pH regarding the pK_a values of the ionisable protons in the isoalloxazine ring. The UV/Vis aborption spectra of the variants **Y193F and Y479F** are also unusual because they lack the peak at 450 nm. This effect is even stronger in Y193F. Since the spectra do not fit to a reduced or oxidized flavin it is hypothesized that these absorption spectra result from an adduct either at the N5 position or C4a of the isoalloxazine ring like detected in hydroperoxyflavin [45]. Since the finding of the alignment of the amino acid sequence from the pfam database assigned to PF08031 in Viridiplantae show that C179 and Y479 are equally conserved it may be assumed that the tyrosine is somehow involved in the cysteinylation of the FAD cofactor. If the cysteinylation is impaired the enzyme is maybe stuck in the reduced state. It is therefore necessary to elucidate the structural properties of these variants by for example X-ray crystallography. It remains unclear why the spectral properties of the enzymes are altered not only in the variants but also in the wild type enzyme.

The characteristic flavin absorption at 380 and 450 nm is less pronounced for the variants **Q438V, Y117F and K438L** as compared to the wild type. Q438V and Y117F show additional maxima that

cannot be assigned to a typical flavin spectrum. Therefore, we hypothesise that the ring system of the cofactor is somehow affected. In the crystal structure of the wild type protein the phenol group of Y117 is located in close distance to the benzyl moiety of the isoalloxazine ring. The loss of the hydroxyl group as well as of its interaction partner Q438 affects the conjugated ring system of the flavin in a comparable manner. Also a small peak at 350 nm is visible, which is also detected in the R292M variant, and is maybe caused by an altered cofactor tethering or by the deprotonation of the oxidized FAD (in the native enzyme or denatured portion).

A single maximum in the absorption spectrum of the denatured WT enzyme was found at approximately 441 nm. The denatured enzyme therefore has its maxima in between one of the stated maxima of 8α-N-histidinylated riboflavin with 445 nm (and 355 nm, was not detected in any spectra of the denatured protein) and the stated maxima of 6-*S*-cysteinylated riboflavin with 437 nm [42]. This is in good accordance with the findings of Winkler *et al*. in the *Ec*BBE. In this study it was also shown that the replacement of the histidine (H104) disrupts the covalent bond leading to a blue shift of the single maximum of the denatured protein [8]. The variants all exhibit a blue shift of their maxima upon denaturation with R292M and Q438V showing a shift of 8 nm the strongest influence on the spectrum of the denatured enzyme compared to the wild type protein. Y479F and Y117F together with N411V and Y193F exhibit maxima similar to the monocovalently bound 6-S-cysteinylated FAD at 437 nm shifted from -1 nm to +2 nm although a second peak at 355 nm did not occur as stated for this kind of bound flavin. A stronger blue shift (-4 nm) compared to 6-*S*-cys FAD is detected in the two variants R292M and Q438V for which also the strongest shift of the maxima compared to the denatured wild type protein is observed. Since these two variants show also unusual peaks at 350 nm in the spectra of the native enzymes it is possible that in these variants the cofactor tethering is somehow impaired.

6.2 pH optima (Figure 10, Figure 11)

Together with **Y193F, Y479F and Q438V, R292M** exhibits of the strongest shift in pH optimum towards 8 compared to the wild type enzyme 7.3. The activity of the enzyme is restored at approximately pH 8 (as was also observed in Y193F, Y479F) which leads to the assumption that the removal of a catalytic base (Y193 or Y479) or the removal of the (partial) positive charge next to Y193 hinders the active site to stabilize the charge necessary for catalysis as well as in the wild type enzyme. In **N411V** the optimum is shifted in the more acidic pH giving rise to the idea that the direct interaction of the positive charge of R292 with Y193 decreases the pK_a of the tyrosine and stabilizes therefore the deprotonated form. **Y117F and K436L** exhibit a pH optimum at 7.8 and 7.5,

respectively. Since they both are hypothesized to stabilize a positive charge in the active site but are assumed as second row residues their shift in the pH optima is rather small.

6.3 pKa values (Figure 10, Figure 11)

Since pK_{a1} and pK_{a2} represent deprotonation events of certain amino acids involved in catalysis it is hypothesized that the lower pK_{a1} represents the deprotonation of Y479 which then can serve as catalytic base to activate Y193 for proton abstraction from the allylic alcohol. Furthermore, the deprotonation of Y193 or of Y117 inhibits catalysis. Y117 seems to be involved in stabilizing the positive partial charge at glutamine 438, which is in close distance to Y193 and Y497. Deprotonation of Y193, in contrast, leads to the disruption of the low barrier hydrogen bond, which results in a reduced enzymatic activity. The **pK_{a1} values** (in more acidic pH) were estimated from the pH at which 50% enzyme activity was left. For the **wild type** protein and **K436L** variant a pK_a of 6.3 was detected. A pK_a of below 6 was detected only for the **N411V** variant, leading to the assumption that N411 is not involved in tuning the pK_a of Y193. R292, in contrast, carries a positive charge, which may indeed stabilize a negative charge at Y193. **Y117F and Y193F** exhibit a p$K_{a1,}$ 6.8, which is only a minor increase compared to the wild type pK_a of 6.3. Both of them are missing a hydroxyl group that can contribute to the H- bonding network in the active site. Therefore, it is assumed that in both cases the pK_a of the Y193-Y479 pair or of Y479 is influenced, since it is believed that the positive charge of Q438 is no longer stabilized in Y117F and therefore a positive charge involved in tuning the pK_a of Y193 (and also Y479) is missing. In the case of Y193F it is supposed that Y479 takes over the role of the tyrosine pair (also possible with Y117 as new interaction partner leaving the Q438 “unbound”). A pK_a of approximately 7 (7.1) was found for **Y479F and R292M** indicating that this value represents the pK_a of Y193 alone, since Y479 is hypothesized to provide a negative charge and R292 provides a positive charge to the catalytic Y193. It is possible that a part of the activity is also restored by introducing Y117 as new interaction partner for Y193 when the hydroxyl group of Y479 is missing. The **Q438V** variants pK_{a1} is 7.8. This is the highest pK_{a1} value detected. Therefore it is hypothesized that the active site of the enzyme is heavily influenced. It is possible that the structurally important Q438 is leaving the catalytic base (Y193) more basic. The **pK_{a2} values** were estimated from the more basic pH at which 50% residual enzyme activity was found. For the **wild type** protein and the **N411V** variant a pK_a of 8.3 was determined. Therefore it is assumed that the deprotonation of Y117 and therefore the loss of the partial positive charge at Q438V is the reason for the decrease in activity. Since it is believed that the replacement of N411V by a valine leads to altered properties of the catalytic Y193-Y479 system, it is however likely that the deprotonation of Y117 is not affected too strongly. A pK_{a2} between 8.8 and 9 was detected for the **Y479F, Y117F and K436L** variant. Since all of

these residues interact with Y193 it is hypothesized that this pK_a values are due to a deprotonation of a tyrosine that is stabilizing the negative charge of the catalytic base. In Y479F it is assumed that Y193 or a restored pair of tyrosines (Y193-Y117) rescues catalysis and therefore the pK_a 9 reflects deprotonation of the more basic tyrosine (Y117) residue. Since in the two latter variants the pK_{a1} is only weakly or not affected it is likely that the pK_{a2} represents the deprotonation of the more basic tyrosine in the catalytic tyrosine pair. It is possible that the loss of Y117 lowers the interaction of Y193-Y479 to a more usual hydrogen bond, leaving maybe the Y193 residue slightly more acidic compared to Y479. Therefore pK_{a2} is believed to reflect the deprotonation of Y479. This would lead to the conclusion that the Y193-Y479 pair pK_as are somehow exchanged and the low barrier hydrogen bond is weakened. In K436L the missing influence on the pK_{a2} is hardly fitting to an explanation. Never the less it is possible that in K436L the low barrier hydrogen bond is still functional and the only property changed in this variant is the pK_a of Y193. A pK_{a2} of more than 9 was found for the **Y193F**, the **R292M**, and the **Q438V** variants. Since all of these are affecting the Y193 residue it is hypothesized that the lysine at position 436 rescues catalysis by donating its positive charge to the active site.

6.4 Turnover numbers

Based on the extinction coefficient of approximately 4960 $M^{-1} \cdot cm^{-1}$ a turnover number of 0.32 s^{-1} was estimated for the wild type *At*BBE-like 15 also determined for k_{cat} in Michaelis-Menten assay with 500 µM cinnamyl alcohol as substrate at the pH optimum. Comparison of the turnover numbers of the active site variants, calculated based on the determined extinction coefficient respectively in contrast to the turnover numbers calculated with the extinction coefficient of the wild type enzyme lead to the conclusion that due to unusual spectroscopic properties of the proteins the calculation with the extinction coefficient determined for the wild type enzyme represent the portion of the active enzyme in a more realistic manner. The estimated relative turnover number of the **N411V** variant is approximately **30%** compared to the wild type enzyme, but in the same range as shown for **K436V (30%)** and **R292M (25%).** This leads to the conclusion that the loss of a partial positive charge (N411) or positive charge (R292) in close vicinity to Y193 or the loss of the cation-π interaction partner (K436) of Y193 strongly influences the catalytic properties of *At*BBE-like 15. The estimated turnover number for the **Y117F** variant is approximately **50%** compared to the wild type enzyme, which is the same range as the residual activity observed with **Y479F (60%).** This leads to the conclusion that a loss of either of these two tyrosine residues has a comparable impact on the catalytic base Y193. In the Y117F variant it is hypothesized that the hydroxyl group is not stabilizing the partial positive charge of Q438 and therefore the negative charge of the catalytic base is

stabilized equally well as in the wild type enzyme. In the Y479F the deprotonation could be performed by Y193 with no (low barrier) hydrogen bond to Y479 or a hydrogen bond is restored with Y117. In both cases the partial positive charge at Q438 is still present. The estimated turnover for the **Y193F** variant is approximately **3%** relative activity compared to the wild type enzyme and the loss of activity is therefore comparable to the **Q483V** (**4%**) variant. This is the greatest loss in activity compared to the turnover numbers of the other variants, which suggests that the removal of the catalytic base Y193 or the partial positive charge of Q438 leads to a more or less catalytically inactive enzyme. It is assumed that in the Q438V variant the active site tyrosines are not held in place and therefore the deprotonation system is not present and/or the alkoxide is not stabilized. The amide portion of Q438 seems to have a more important role than the amide portion of N411 in close vicinity of Y193. Since N411 is interacting with R292 it is also possible that in the N411V variant the arginine is compensating the missing positive charge by moving towards the catalytic tyrosines.

6.5 *At*BBE-like 26

All attempts to produce the His-tagged protein in *K. phaffii* did not lead to any active protein. However, western blot analysis revealed that at least a His-tagged protein was transcribed, although, secretion to the culture medium was not successful. Disruption of the cells using a Merckenschlager disintegrator, followed by affinity chromatography, did not lead to a purified protein with the typical absorption characteristics of a flavoprotein.

6.6 Experimental approach

The approach of Michaelis and Menten is used to determine the rates of the conversion of the product at different substrate concentrations. The hyperbolic plot obtained when plotting these rates as a function of the respective substrate concentration allows the determination of a limiting rate (v_{max}, k_{cat}) as well as of a K_M value. It is assumed that the corresponding substrate concentration is sufficient for the entire enzyme to be present in its substrate bound complex [ES], the Michaelis Menten complex, which causes the turnover to be solely dependent on the conversion of the bound substrate into the product giving rise to the enzyme product complex [EP] and in the next step the release of the product. The Michaelis Menten constant K_M is giving the substrate concentration at the half maximal velocity of the enzyme and is representing the affinity of the enzyme to the respective substrate.

For *At*BBE-like 15 allylic alcohols were tested as substrate especially as described before the natural occurring monolignols sinapyl alcohol, coumaryl alcohol, coniferylalcohol. One not naturally occurring substrate analogon is cinnamyl alcohol with very similar structure to the monolignols but

missing substituents on the benzyl ring. It was revealed that the monolignols could not be used in steady state assay as the reaction rates exceeded the limit of detection. Moreover, inhibition was observed and/or the oxidative half reaction was found to be the rate-limiting step. Nevertheless in pre-steady state kinetics under anaerobic conditions we were able to use coniferyl alcohol as a substrate to elucidate information on the transient kinetics of the enzyme. With cinnamyl alcohol the rate of the reaction was in a proper range for studies under steady state conditions, but tested in pre-steady state approach no limiting rate was observed up to 5 mM substrate, which is reflected by the linear plot shown in Figure 14. This gives rise to the idea that substrate binding is impaired if the hydroxyl or methoxy groups at the aromatic ring are missing.

When we first tested our enzyme in steady state approach toward its pH optimum with 1000 µM of coniferyl alcohol as a substrate it was evaluated, that this concentration was far in the range of enzyme saturation. The pH optimum was determined at pH 5 which was not correlating to the former findings of Pils *et al*. for the *At*BBE-like 15 L182V variant designed as an oxidase for the electron transfer to molecular oxygen [46]. Therefore cinnamyl alcohol was tested in Michaelis-Menten approach and it was found that a substrate concentration of 500 µM cinnamyl alcohol gives the half maximal rate for the conversion of the substrate and therefore this condition was chosen to make sure that the reductive half reaction of the enzyme is the visible rate limiting step in this experimental setup. Although this suitable concentration of the substrate was determined for the wild type enzyme it remains unclear if the variants exhibit different hyperbolas for in the steady state assay with increasing substrate concentrations and if the hyperbola of the wild type enzyme is not influenced by a pH change.

It is stated that the effect of pH on v_{max} is reflected by a bell shaped, symmetric curve with an optimum in a certain pH range. It is further stated that the pK_a is reflected at the pH which the velocity has half its maximum value. [47], [48]. Since we were not able to follow the reaction at v_{max} due to the slow oxidative half reaction is questionable if we were able to catch the pH optimum since not the entire enzyme is in the active enzyme-substrate complex with 500 µM cinnamyl alcohol.

It is important to evaluate the overall reaction on the rate limiting step as in some point other rates as for example the oxidative half reaction or DCPIP reduction is the slowest step and therefore the rate of the reductive half reaction of the enzyme is hidden. Nevertheless in this experimental approach it is necessary to keep in mind that the values determined are only the apparent values in

respect to the complexity of the assay and the unrevealed properties of the electron transfer to DCPIP.

7 Conclusion

We successfully produced a set of stable AtBBE-like 15 variants and we were able to purify them. Their unexpected UV/VIS absorption spectra are not easy to interpret and need further examination. Since the spectra of the denatured enzymes are rather similar, it is likely the exchange of amino acids in the active site affects the flavin ring system. Furthermore, the determination of the catalytic properties of the variants showed a significant decrease in activity and a shift in the pH optima for residues proposed to directly take part in the catalysis directly. In conclusion our hypothesis of the proton abstraction by a catalytic base and the stabilization of the alkoxide by the amides, together with the guanidinium group of R292, prior to the formation of the aldehyde could neither be proven nor rejected.

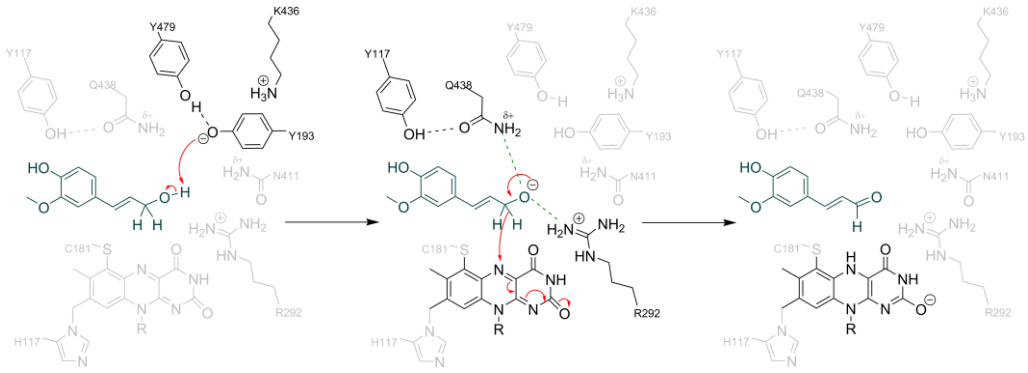

Scheme 4: Proposed reaction mechanism. The substrate is deprotonated by the catalytic base Y193. The corresponding alkoxide is stabilized by the (partial) positive charges of R292 and Q438 in the active site prior to the hydride transfer to the flavin cofactor and formation of the aldehyde product.

8 References

[1] P. Macheroux, B. Kappes, and S. E. Ealick, “Flavogenomics - a genomic and structural view of flavin-dependent proteins,” *FEBS J.*, vol. 278, no. 15, pp. 2625–2634, Aug. 2011.

[2] D. P. H. M. Heuts, N. S. Scrutton, W. S. McIntire, and M. W. Fraaije, “What’s in a covalent bond?,” *FEBS J.*, vol. 276, no. 13, pp. 3405–3427, Jun. 2009.

[3] M.-H. Lee, W.-L. Lai, S.-F. Lin, C.-S. Hsu, S.-H. Liaw, and Y.-C. Tsai, “Structural Characterization of Glucooligosaccharide Oxidase from Acremonium strictum,” *Appl. Environ. Microbiol.*, vol. 71, no. 12, pp. 8881–8887, Dec. 2005.

[4] J. Jin, H. Mazon, R. H. H. van den Heuvel, A. J. Heck, D. B. Janssen, and M. W. Fraaije, “Covalent flavinylation of vanillyl-alcohol oxidase is an autocatalytic process,” *FEBS J.*, vol. 275, no. 20, pp. 5191–5200, Oct. 2008.

[5] B. Daniel *et al.*, “The family of berberine bridge enzyme-like enzymes: A treasure-trove of oxidative reactions,” *Arch. Biochem. Biophys.*, vol. 632, pp. 88–103, Oct. 2017.

[6] A. Winkler, T. M. Kutchan, and P. Macheroux, “6- S -Cysteinylation of Bi-covalently Attached FAD in Berberine Bridge Enzyme Tunes the Redox Potential for Optimal Activity,” *J. Biol. Chem.*, vol. 282, no. 33, pp. 24437–24443, Aug. 2007.

[7] A. Winkler, F. Hartner, T. M. Kutchan, A. Glieder, and P. Macheroux, “Biochemical Evidence That Berberine Bridge Enzyme Belongs to a Novel Family of Flavoproteins Containing a Bi-covalently Attached FAD Cofactor,” *J. Biol. Chem.*, vol. 281, no. 30, pp. 21276–21285, Jul. 2006.

[8] A. Winkler, K. Motz, S. Riedl, M. Puhl, P. Macheroux, and K. Gruber, “Structural and Mechanistic Studies Reveal the Functional Role of Bicovalent Flavinylation in Berberine Bridge Enzyme,” *J. Biol. Chem.*, vol. 284, no. 30, pp. 19993–20001, Jul. 2009.

[9] B. Daniel *et al.*, “Structure of a berberine bridge enzyme-like enzyme with an active site specific to the plant family Brassicaceae,” *PLoS One*, 2016.

[10] I. Letunic and P. Bork, “Interactive tree of life (iTOL) v3: an online tool for the display and annotation of phylogenetic and other trees.,” *Nucleic acids research*. p. gkw290-, 2016.

[11] R. H. H. Van Den Heuvel, M. W. Fraaije, A. Mattevi, C. Laane, and W. J. H. Van Berkel, “Vanillyl-alcohol oxidase, a tasteful biocatalyst,” in *Journal of Molecular Catalysis - B Enzymatic*, 2001, vol. 11, no. 4–6, pp. 185–188.

[12] F. Scott Mathews, Z. W. Chen, H. D. Bellamy, and W. S. McIntire, “Three-Dimensional Structure of p-Cresol Methylhydroxylase (Flavocytochrome c) from Pseudomonas putida at 3.0-Å Resolution,” *Biochemistry*, 1991.

[13] Q. T. Nguyen, G. de Gonzalo, C. Binda, A. Rioz-Martínez, A. Mattevi, and M. W. Fraaije,

"Biocatalytic Properties and Structural Analysis of Eugenol Oxidase from Rhodococcus jostii RHA1: A Versatile Oxidative Biocatalyst," *ChemBioChem*, pp. 1359–1366, 2016.

[14] T. Schmülling, T. Werner, M. Riefler, E. Krupková, and I. Bartrina Y Manns, "Structure and function of cytokinin oxidase/dehydrogenase genes of maize, rice, Arabidopsis and other species," in *Journal of Plant Research*, 2003.

[15] N. Noinaj *et al.*, "The crystal structure and mechanism of an unusual oxidoreductase, GilR, involved in gilvocarcin V biosynthesis," *J. Biol. Chem.*, 2011.

[16] J. C. Carlson *et al.*, "Tirandamycin Biosynthesis is Mediated by Co-Dependent Oxidative Enzymes," *Nat.Chem*, vol. 3, p. 628, 2011.

[17] Y. S. Li *et al.*, "A unique flavin mononucleotide-linked primary alcohol oxidase for glycopeptide A40926 maturation," *J. Am. Chem. Soc.*, 2007.

[18] A. Sultana, I. Alexeev, I. Kursula, P. Mäntsälä, J. Niemi, and G. Schneider, "Structure determination by multiwavelength anomalous diffraction of aclacinomycin oxidoreductase: Indications of multidomain pseudomerohedral twinning," *Acta Crystallogr. Sect. D Biol. Crystallogr.*, 2007.

[19] A. Sultana, J. Niemi, P. Mantsala, G. Schneider, and I. Alexeev, "Aclacinomycin oxidoreductase (AknOx) from the biosynthetic pathway of the antibiotic aclacinomycin is an unusual flavoenzyme with a dual active site," *Proc. Natl. Acad. Sci.*, 2007.

[20] R. Teufel *et al.*, "Flavin-mediated dual oxidation controls an enzymatic Favorskii-type rearrangement.," *Nature*, vol. 503, pp. 552–556, 2013.

[21] J. W. A. Koetter and G. E. Schulz, "Crystal Structure of 6-Hydroxy-D-Nicotine Oxidase from Arthrobacter Nicotinovorans.," *J.Mol.Biol.*, vol. 352, p. 418, 2005.

[22] A. R. Ferrari *et al.*, "Discovery of a Xylooligosaccharide Oxidase from Myceliophthora thermophila C1.," *J.Biol.Chem.*, vol. 291, pp. 23709–23718, 2016.

[23] J. Duskova *et al.*, "Crystal structure and kinetic studies of carbohydrate oxidase from Microdochium nivale," *TO BE Publ.*

[24] N. Lorenz, E. V. Wilson, C. Machado, C. L. Schardl, and P. Tudzynski, "Comparison of Ergot Alkaloid Biosynthesis Gene Clusters in Claviceps Species Indicates Loss of Late Pathway Steps in Evolution of C. fusiformis," *Appl. Environ. Microbiol.*, vol. 73, no. 22, pp. 7185–7191, Nov. 2007.

[25] M. Kamimura *et al.*, "Fungal ecdysteroid-22-oxidase, a new tool for manipulating ecdysteroid signaling and insect development," *J. Biol. Chem.*, 2012.

[26] M. Toplak *et al.*, "The single berberine bridge enzyme homolog of Physcomitrella patens is a cellobiose oxidase," *FEBS J.*, vol. 285, no. 10, pp. 1923–1943, May 2018.

[27] B. Daniel *et al.*, “Oxidation of monolignols by members of the berberine bridge enzyme family suggests a role in plant cell wall metabolism,” *J. Biol. Chem.*, vol. 290, no. 30, pp. 18770–18781, Jul. 2015.

[28] J. Rajniak, B. Barco, N. K. Clay, and E. S. Sattely, “A new cyanogenic metabolite in Arabidopsis required for inducible pathogen defence,” *Nature*, vol. 525, pp. 375–379, 2015.

[29] J. H. H. V Custers *et al.*, “Isolation and characterisation of a class of carbohydrate oxidases from higher plants, with a role in active defence,” *Plant J.*, vol. 39, pp. 147–160, 2004.

[30] M. Kajikawa, T. Shoji, A. Kato, and T. Hashimoto, “Vacuole-localized berberine bridge enzyme-like proteins are required for a late step of nicotine biosynthesis in tobacco.,” *Plant Physiol.*, vol. 155, no. 4, pp. 2010–22, Apr. 2011.

[31] Y. Shoyama *et al.*, “Structure and function of 1-tetrahydrocannabinolic acid (THCA) synthase, the enzyme controlling the psychoactivity of Cannabis sativa,” *J.Mol.Biol.*, vol. 423, pp. 96–105, 2012.

[32] A. Winkler, M. Puhl, H. Weber, T. M. Kutchan, K. Gruber, and P. Macheroux, “Berberine bridge enzyme catalyzes the six electron oxidation of (S)-reticuline to dehydroscoulerine,” *Phytochemistry*, vol. 70, no. 9, pp. 1092–1097, Jun. 2009.

[33] D. Zafred, A. Nandy, L. Pump, H. Kahlert, and W. Keller, “Crystal structure and immunologic characterization of the major grass pollen allergen Phl p 4.,” *J. Allergy Clin. Immunol.*, vol. 132, p. 696–703.e10, 2013.

[34] T. H. Huang, H. J. Peng, S. N. Su, and S. H. Liaw, “Various cross-reactivity of the grass pollen group 4 allergens: crystallographic study of the Bermuda grass isoallergen Cyn d 4.,” *Acta Crystallogr.,Sect.D*, vol. 68, pp. 1303–1310, 2012.

[35] J. J. Almagro Armenteros *et al.*, “SignalP 5.0 improves signal peptide predictions using deep neural networks,” *Nat. Biotechnol.*, p. 1, Feb. 2019.

[36] P. Artimo *et al.*, “ExPASy: SIB bioinformatics resource portal,” *Nucleic Acids Res.*, vol. 40, no. W1, pp. W597–W603, Jul. 2012.

[37] “UniProt: a worldwide hub of protein knowledge,” *Nucleic Acids Res.*, vol. 47, no. D1, pp. D506–D515, Jan. 2019.

[38] J. P. Klinman, “Low Barrier Hydrogen Bonds: Getting Close, but Not Sharing...,” *ACS Cent. Sci.*, vol. 1, no. 3, pp. 115–116, Jun. 2015.

[39] W. W. Cleland, P. A. Frey, and J. A. Gerlt, “The low barrier hydrogen bond in enzymatic catalysis.,” *J. Biol. Chem.*, vol. 273, no. 40, pp. 25529–32, Oct. 1998.

[40] W. W. Cleland, “Low-Barrier Hydrogen Bonds and Enzymatic Catalysis,” *Arch. Biochem. Biophys.*, vol. 382, no. 1, pp. 1–5, Oct. 2000.

[41] C.-H. Wu, K. Ito, A. M. Buytendyk, K. H. Bowen, and J. I. Wu, “Enormous Hydrogen Bond Strength Enhancement through π-Conjugation Gain: Implications for Enzyme Catalysis,” *Biochemistry*, vol. 56, no. 33, pp. 4318–4322, Aug. 2017.

[42] S. K. Chapman and G. A. Reid, *Flavoprotein Protocols*, vol. 131. New Jersey: Humana Press, 1999.

[43] J. McD. Armstrong, “The molar extinction coefficient of 2,6-dichlorophenol indophenol,” *Biochim. Biophys. Acta - Gen. Subj.*, vol. 86, no. 1, pp. 194–197, Apr. 1964.

[44] J. Galbán, I. Sanz-Vicente, J. Navarro, and S. de Marcos, “The intrinsic fluorescence of FAD and its application in analytical chemistry: a review,” *Methods Appl. Fluoresc.*, vol. 4, no. 4, p. 042005, Dec. 2016.

[45] K. Crozier-Reabe and G. Moran, “Form Follows Function: Structural and Catalytic Variation in the Class A Flavoprotein Monooxygenases,” *Int. J. Mol. Sci.*, vol. 13, no. 12, pp. 15601–15639, Nov. 2012.

[46] S. Pils *et al.*, “Characterization of the monolignol oxidoreductase AtBBE-like protein 15 L182V for biocatalytic applications,” *J. Mol. Catal. B Enzym.*, 2016.

[47] S. Ainsworth, *Steady-State Enzyme Kinetics*. London: Macmillan Education UK, 1977.

[48] R. A. Alberty and V. Massey, “On the interpretation of the pH variation of the maximum initial velocity of an enzyme-catalyzed reaction,” *Biochim. Biophys. Acta*, vol. 13, pp. 347–353, Jan. 1954.

9 APPENDIX